Scuola Internazionale Superiore di Studi Avanzati - Trieste

Combining calcium imaging with optogenetics in hippocampal primary cultures

Thesis submitted for the degree of “Doctor Philosophiae”

Academic year 2017/2018

PhD in Neurobiology

November 2018

Candidate
Fiamma Romagnoli

Supervisor
Vincent Torre

Per aspera ad astra.

INDEX

DECLARATION

All the work described in this thesis arises exclusively from my own experiments. I carried out both the experimental work and the analysis of the data. Experiments were performed at the International School for Advanced Studies, SISSA, under the supervision of Professor Vincent Torre.

ABSTRACT

Calcium imaging and optogenetics are two powerful tools in neuroscience research. Their combination can give great insights on the working of neural networks and circuits and can complement electrophysiological data.

The present investigation shows that it is possible to analyse neuronal networks with optogenetic tools *in vitro*, where light is used to open and close ionic channels that have conduction properties identical to native channels. In this project we have opted for the optogenetic approach of Photoisomerizable Tethered Ligands (PTL). By tethering synthetic photoisomerizable compounds (PTLs, also called *photoswitches*) to engineered native proteins (channels or receptors), we gain the possibility of controlling them with light. In our case, these engineered proteins were ionotropic kainate-type glutamate receptors, called LiGluK2.

In rat primary hippocampal cultures, we combined the optical stimulation of LiGluK2 with optical sensing by means of calcium imaging. Localized activation of LiGluK2 with confined illumination allowed us to control single neurons and analyse the effect of their activation on small neural networks. Different stimulation protocols were applied, and we found transfected neurons to have mainly three different kinds of responses in terms of calcium transients: single peaks, single prolonged calcium transients, multiple peaks. This activity affected surrounding neurons with variability, which can be ascribed to the physiological properties of the neurons involved and to the random connectivity of the analysed neural networks.

AIM OF THE STUDY

The aim of the study was to combine calcium imaging with optogenetics *in vitro* in hippocampal primary cultures.

The optical tool we considered was the Photoisomerizable Tethered Ligand (PTL) approach, where photoisomerizable synthetic compounds (PTLs, also called *photoswitches)* are tethered to engineered native proteins, allowing to control their activity with light. Among the existing PTL-based strategies, we decided to work with LiGluK2, which is based on the native kainate receptor GluK2, and, apart from its optical controllability, maintains all its key aspects. GluK2 plays distinct roles at excitatory and inhibitory synapses throughout the brain and has been implicated in a variety of neurological diseases, including mood disorders and epilepsy [1,2]. Compared to classical optogenetic approaches that use opsins, the PTL strategy allows us not only to control cellular excitability, but to eventually probe the function of specific receptor subtypes, both *in vitro* and *in vivo*, with unprecedented resolution.

The objective was to transfect LiGluK2 and measure the electrical activity of primary cell culture networks with calcium imaging, combining optical stimulation with optical sensing. The optical activation of single transfected neurons would allow us to have control on the activity of small networks of neurons. To do this, we chose a red-shifted calcium dye, Rhod-3 AM, characterized by very close excitation and emission peaks (ex/em 560/600 nm), to perform calcium imaging during LiGluK2 activation. To simplify activation and inactivation of the photoswitch, we decided to try to use the calcium imaging light to deactivate the receptor, limiting the time of activation of the receptor to the time of illumination with the UV stimulus. The confinement of the stimulus by means of an optical fibre would allow to briefly activate the receptors and visualize the effect of this controlled activation on surrounding neurons.

One of the most interesting features of the PTL-based approach, is that engineering of the native proteins does not alter their capability of binding PTLs. This means that, knowing the structure of the protein, it is possible to mutate single residues in functional and regulatory sites and directly test their effects on cellular function. The first step after mutation would be to screen points of attachment for the PTL, and the fastest way to assay them is through calcium imaging [3]. Our method could then be combined with electrophysiological recordings and give a major insight on the effects of single mutations

introduced in ionotropic/metabotropic glutamate or GABA receptors developed as light-gated receptors [4,5].

INTRODUCTION

OPTOGENETICS AND OPTICAL METHODS

Optogenetics has had a strong impact on neuroscience. It is an innovative technique for optically controlling cellular activity. This field has exploded over the past decade or so and has given rise to great advances in the field [6].

Optogenetics is a photostimulation technique in which the light-sensitive target is introduced genetically [7]. It refers to the combined use of optics and genetics with the aim of controlling the functions of genetically modified target cells. These functions can be gene activation, intracellular signalling and stimulation/inhibition of cells. This makes optogenetics an advantageous tool in studying and manipulating cellular systems.

The outstanding features of this technique are cellular specificity and high temporal resolution: neurons may be controlled with optogenetics for fast, specific excitation or inhibition within systems as complex as freely moving mammals [8]. Using hetereologously expressed light-sensitive opsins, be it G protein-coupled receptors, ion channels or pumps, optogenetics has made it possible to stimulate or inhibit activity in selected neurons, allowing us to probe the role of these cells in circuit function or behaviour [7].

In addition to naturally light-sensitive opsins used in “classic” optogenetics, chemical synthesis combined with protein engineering has produced a complementary “chemical” optogenetics, also known as photopharmacology [9] or optogenetic pharmacology [10]. Chemical synthesis is combined with protein engineering with the aim of modifying native mammalian channels, as well as ionotropic and metabotropic receptors. This means that we can modify native receptors endowing them with sensitivity to light. In this way they can be blocked, agonized or antagonized by light, and pre-synaptic or post-synaptic neuronal responses to neurotransmitter release can be selectively controlled.

We can classify optogenetic methods in two main categories (Figure 1):

A. **Classic Optogenetics**: heterologous expression of naturally light-sensitive proteins (opsins).

B. **Chemical Optogenetics** (also called optopharmacology): native mammalian channels and receptors are engineered to be controlled by light.

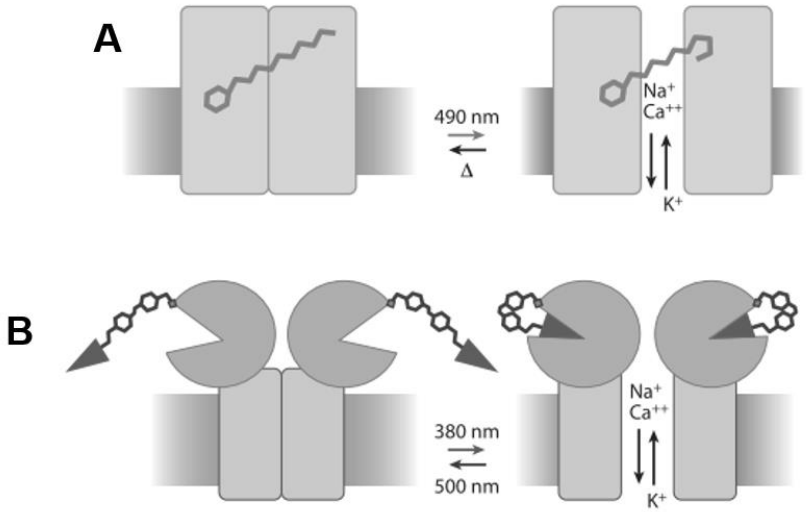

Figure 1: Classic and Chemical Optogenetics. A. Classic Optogenetics: Opsins (light-gated ion channels) are naturally sensitive to light and can be expressed in neurons; these proteins interact with the chromophore retinal, native to the nervous system of many animals, to photoregulate the membrane potential. **B. Chemical Optogenetics**: Neurotransmitter receptors can be engineered to become light sensitive when coupled to a synthetic photoswitchable molecule containing an analogue of the native neurotransmitter (figure from Szobota & Isacoff, 2010 [7]).

Classic Optogenetics

Traditional optogenetics involves the introduction of genes encoding light-sensitive transmembrane ion conductance regulators (most commonly microbial opsins) to enable excitation or inhibition of targeted cells, with the biological effect depending on the opsin employed (Figure 1A). Many opsins with distinct properties are used in optogenetics, with the most widely utilized being a mammalian codon-optimized

channelrhodopsin (ChR2) and a third-generation halorhodopsin optimized for membrane trafficking in mammalian cells (eNpHR3.0)[11].

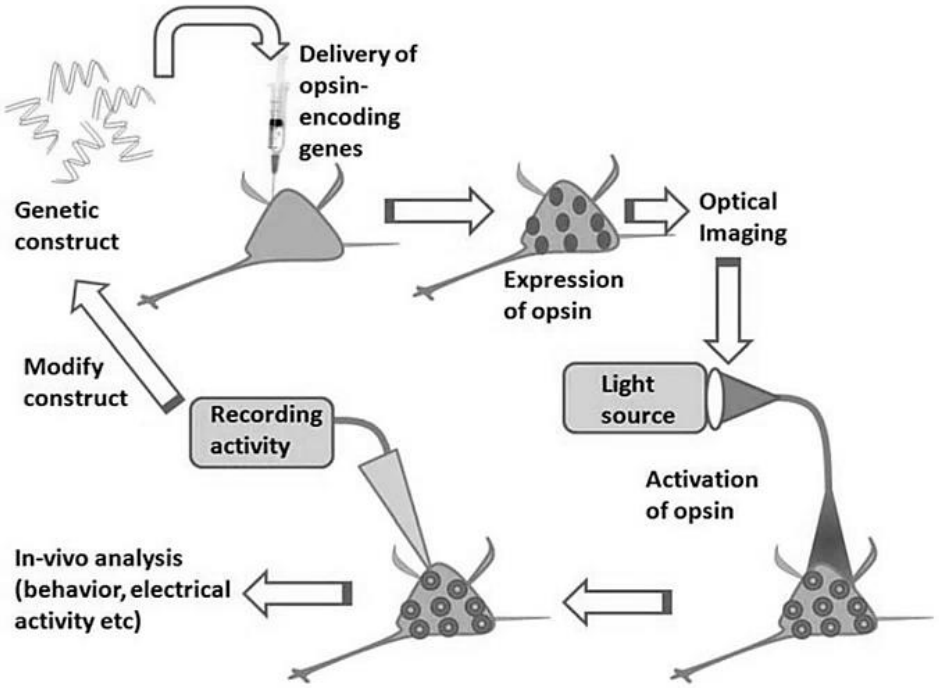

Figure 2: Intuitive description of the optogenetic stimulation method. Synthesis of the genetic construct encoding for the opsin, delivery and expression of opsins in targeted cells, optical activation of opsin-expressing cells followed by readout, modification of construct to obtain better optical control [12].

Opsins

Opsin genes are divided in two distinct superfamilies: microbial opsins (type I) and animal opsins (type II). Type I opsin genes are found in prokaryotes, algae, and fungi [13], while type II are present only in higher eukaryotes and are responsible for vision, primarily, but are also involved in circadian rhythm and pigment regulation [14,15]. Moreover, while type II opsin genes encode for G protein-coupled receptors, type I genes code for ionotropic receptors. Even though both types of genes codify for 7-transmembrame-helix proteins, there is a very low sequence homology between the two superfamilies.

Opsin proteins from both families require retinal, a vitamin A-related organic cofactor that serves as an antenna for photons; when retinal is bound, the functional opsin proteins are termed rhodopsins. Retinal covalently binds to a conserved lysine residue of the seventh helix by forming a protonated retinal Schiff base (RSBH+). The ionic environment of the RSB, defined by the residues of the binding pocket, dictates the spectral and kinetic characteristics of each individual protein. Retinal isomerizes upon the absorption of a photon, consequently triggering a sequence of conformational changes within the opsin partner and initiating its activity [8].

Channelrhodopsins are a subfamily of retinylidene proteins that function as light-gated ion channels [16]. Channelrhodopsin-2 (ChR2) is an important photochemical switch responsible for the phototaxic nature of algae *Chlamydomonas reinharditii*. In a pigmented organelle called eyespot, which helps the *Chlamydomonas* swim towards the light, we can find the Channelrhodopsin-2 protein, which is a cation channel. In the presence of the chromophore all-trans-retinal (ATR), ChR2 is activated with ms-kinetics by a band of blue light (λ=440-500 nm) with intensity threshold less than 1mW/mm^2 [12].

In 2003, Nagel *et al.* showed for the first time that ChR2 can be used to depolarize cells (mammalian HEK cells and *Xenopus laevis* oocytes) upon blue light illumination with high temporal precision [16]. Subsequently, *in vitro* optogenetic activation of neurons using ChR2 was demonstrated, thus becoming the first single-component optogenetic tool [17]. In addition to stimulation, silencing of neurons has been reported using a chloride channel based halorhodospin(NpHR) [18,19]. Since the activation peak of halorhodopsin is in the yellow spectral range, combination of the two channels can be used for optical stimulation and silencing of neural activity with high temporal resolution.

Gene Delivery and Expression

The first step in using ChR2 (or other opsins) in neurons is to create a genetic construct encoding the opsin and targeting it to neurons by mean of a cell-specific promoter. In addition to this, since opsins are not fluorescent, the plasmid

encoding ChR2 must be fused with a sequence codifying for a fluorescent reporter protein for visualizing its expression in cells.

Construct delivery can be done both with viral and non-viral methods:

- **Viral methods**

  Adeno-associated virus (AAV) or lentivirus are generally used to package the genetic construct and deliver it near the neurons, in a petri dish or stereotactically into the brain region of interest [20]. Lentiviral vectors confer permanent expression of the genetic construct since they are integrated into the genome of the target cell [21]. AAV-mediated expression, on the other hand, may be less stable due to the fact that a much smaller percentage of the virus is integrated.

- **Non-viral methods**

  Include lipofection, electroporation, and optoporation. Lipofection, also known as "lipid transfection" or "liposome-based transfection", uses a lipid complex to deliver DNA to cells. This technology uses tiny vesicular structures called liposomes that have the same composition as the cell membrane. Depending on the liposome and cell type, the liposome can be endocytosed or directly fuse with the cell membrane to release the DNA construct into cells. The advantage to lipofection is that it works in many cell types, but is almost exclusively used in cell culture experiments [22].

  Electroporation is the process of using an electric pulse to transfect cells with DNA. Applying an electric field to cells is thought to induce temporary pores in the cell membrane, allowing the cell to take up DNA sequences. After the electric field is switched off, the cell membrane reseals, trapping some of the electroporated DNA within the cell. Electroporation can be used to efficiently deliver DNA to cells for *in vitro* conditions. In neuroscience research, electroporation has been particularly useful for *in utero* preparations [22].

  In the last two decades, laser-assisted cellular poration (also called photoporation, optoporation or laserfection) has been utilized to efficiently introduce macromolecules into intact cells. By using a tightly focused laser beam, the cell membrane can be perforated in a highly controlled manner, allowing exogenous molecules to enter the cell. Femtosecond (fs) near–infrared laser based transfection has been shown to be safe, providing high

efficiency and survival (93%) of optoporated embryo during development [23], as well as for in-vivo gene delivery [24] as opposed to electroporation [12].

Animal models

In addition to these delivery methods, transgenic animals expressing tissue-specific opsins have been developed: *Caenorhabditis elegans*, *Drosophila*, zebrafish, mice, rats and primates. Using these transgenic or knock-in animals allows greater control of transgene expression by using larger promoter fragments and obviates viral payload limitations, but their use requires time, effort, and cost associated with their production, validation, and maintenance [8].

Caenorhabditis elegans

Mechanosensory neuron activity and muscle wall motor neuron can be controlled in transgenic nematodes harbouring the channelrhodopsin gene [16]. Combinatorial optogenetics has also been used to bidirectionally control body wall muscle contraction by expressing ChR2 and NpHR [19]. *C. elegans* was also used for combined light-based stimulation and readout of neural activity [25,26], fulfilling the promise of all-optical physiological experiments using optogenetic tools and genetically encoded activity sensors [27].

Drosophila

Drosophila flies have been used to investigate appetitive/aversive odorant learning both at the receptor and neurotransmitter levels [28,29], the neuronal basis of the nociceptive response [30] and to rescue photosensory mutants [31]. These fly lines express an upstream activation sequence for channelrhodopsin2 (UAS-ChR2) [32]. Moreover, special considerations are required for this model organism [33]. One thing that must be considered in the use of flies and worms is that, unlike mammals, they do not possess levels of endogenous retinal that are sufficient for the functioning of optogenetic tools. Food supplement, however, can provide

enough retinal to drive ChR2 function [31]. In addition to this, flies possess an innate behavioral response to blue light that is developmentally dependent [28,31]. This complicates behavioral studies that use opsins activated in the blue spectra. This problem, in theory, could be bypassed using red-shifted optogenetic tools for excitation and inhibition. Spiking may be driven with up to 630 nm light, improving the potential for deep-penetrating excitation [33].

Zebrafish

The main advantages in using zebrafish for optogenetics are the short generational time and easy integration of foreign DNA, plus the facilitated genetic manipulation due to the transparency of the organism [34,35]. The first time optogenetic tools were used in zebrafish was in a study which examined the role of somatosensory control of escape behavior, where ChR2 was used to drive single spikes in a genetically defined population during the course of movement [36]. In the case of zebrafish, in addition to stable transgenic lines it is also possible to express the ChR2 gene by means of viral infection. This has been done by Zhu *et al.* in 2009 by using the Sindbis and rabies viruses [37].

Mouse

To date, the mouse is the most extensively published optogenetic model organism and represents the majority of transgenic animals.

The first transgenic opsin-expressing mouse line was generated using the Thy1 promoter [38,39] with widespread expression throughout the cortical layer 5 projection neurons as well as in some subcortical structures [38]. This mouse line has been widely used, for example, to examine the roles of inhibitory neurons on cortical information processing [40]. Subsequently, several other groups have also generated transgenic mouse lines directly expressing opsin genes [41–43]. Optogenetics in this model has also been used to study possible therapeutic mechanisms of cortical intervention in mouse models of depression [44] and to shed light on fear and anxiety behaviors by studying amygdala circuits [45–47]. These last

studies in particular have shown how complex behaviors can be dissected with optogenetic tools.

Rat

Their ability to perform complex behavioral tasks, the relative simplicity of their brains compared with human and nonhuman primates, and the ability to perform high density neural recordings in the free behaving animal, makes the rat an important model for neuroscience research. But optogenetic research in rats is limited by the availability of viral promoters capable of driving specific expression in the absence of transgenic targeting. However, transgenic rat lines expressing Cre recombinase in specific neuronal subtypes will greatly expand the potential for using rat models of neural circuit function in health and disease [8].

Primates

ChR2 delivery to cortical neurons via lentiviral transduction has been achieved in macaques, but behavioral responses have not yet been observed [48,49]. In humans, eNpHR2.0, in the form of ex vivo human retinas, was delivered to human neural tissue and optogenetic efficacy on physiological measures was shown [50]. This has possible relevance to retinitis pigmentosa (RP), a disease where light-sensing cells in the retina degenerate, since the expression of eNpHR2.0 in light-insensitive cone cells restored normal phototransduction.

Methods for confirming the expression of the opsin in the targeted cells vary on the basis of *in vitro* or *in vivo* experiments. In *in vitro* experiments, expression is verified by visualizing the fluorescence reporter protein by means conventional epifluorescence microscopy. In *in vivo* experiments, on the other hand, methods will vary according to the animal model employed. In the case of mammals, for example, confocal or multiphoton microscopy can be used in superficial brain regions with a special arrangement (for example an optical window on the dura mater, with skull removed) with single cell resolution. Conversely, the sacrifice of the animal after the experiments is necessary for deeper brain regions. In this

case, slices of the brain are performed after the sacrifice and opsin expression can be assessed with confocal microscopy with no additional staining. For correlating opsin expression with specific cell types immunohistochemistry is required: antibodies for opsins and target cells are used and co-localization is verified with confocal fluorescence microscopy [12].

Illumination and readout of optogenetic experiments

Controlled optical activation of opsin-expressing cells is achieved with different illumination parameters. First of all, the wavelength of the light sources must be considered, and must generally match the maximum activation peak of the opsin. Secondly, temporal control of the light pulses is necessary for controlling and probing neurons.

Patch clamp recordings are generally carried out *in vitro* to measure intra-cellular currents or generation/inhibition of action potentials by light activation. Other methods to detect stimulation/inhibition of neurons by optogenetic activation include single metallic electrodes or arrays of multiple electrodes and fluorescence biosensors such as calcium dyes. All these methods have been used both *in vivo* and *in vitro*, but as far as *in vivo* goes, another crucial factor to consider is the animal's behaviour following optogenetic stimulation/inhibition, which allows us to evaluate the overall outcome of the optogenetic manipulation. All experimental read out values will then help modify the optogenetic construct and the experimental parameters in order to obtain better optical control of the targeted neurons and of the overall function of the neural circuitry [12].

Chemical Optogenetics: Optopharmacology

With chemical optogenetics, native mammalian channels, ionotropic, and metabotropic receptors can be blocked, agonized, or antagonized by light, enabling presynaptic or postsynaptic neuronal responses to neurotransmitter release to be selectively controlled [5,51].

An example of this strategy is Photoisomerizable Tethered Ligands (Figure 1B), which bind to genetically engineered channels or receptors and allow to control them

with light. Proteins are engineered by introducing a cysteine point mutation near their ligand-binding domain (LBD) that creates a point of attachment for a cysteine-reactive PTL. These proteins can then be targeted to particular neurons or cellular regions by using specific promoters or signalling motifs [7]. We decided to use this strategy in our experiments.

PTLs are photoisomerizable synthetic compounds with a modular structure. This makes it possible to sculpt the optical control element by designing each of its modules. The general structure of PTLs is:

- **Reactant**: reactive group that mediates the covalent attachment to the target protein near the its binding site.
- **Linker**: photoisomerizable linker that changes conformation with light
- **Ligand**: agonist, antagonist, blocker

The photoisomerizable linker is the crucial part of PTLs. By means of a mechanism called photoswitching [8], the linker switches between two isomers when illuminated by two different wavelengths of light, and either presents or removes the ligand from its binding site. This is why these linkers are also called *photoswitches*. Several chemical groups can be utilized in this way [9], such as spiropyrans [10], thioamids [11], and azobenzenes.

Azobenzene derivatives are the most popular photoswitches, since they have excellent photophysical properties and allow robust and efficient switching [12,13]. Azobenzene's shape and end-to-end length change significantly when the molecule shifts between its elongated *trans* form to its compact *cis* form. The peak absorption wavelengths that drive the molecule between the two configurations are spectrally well separated, typically 380 (*trans* to *cis*) and 500 nm (*cis* to *trans*), depending on the nature of the substituents attached to the azobenzene [3]. In the dark azobenzene is in a stable *trans* configuration, while light between 370-390 nm causes it to "bend" into the higher energy *cis* isomer. To efficiently turn azobenzene back to its *trans* isomer, 480–530 nm light can be used (>85 % *trans*). Wavelengths >530 nm favor the *trans* configuration as well, but the absorption becomes weak and photoswitching requires increasingly more light [10]. Even compared to other optical techniques, PTLs allow particularly precise spatiotemporal control since the photoisomerization of azobenzene is a picosecond process and binding is not limited by diffusion [52].

SPARK and D-SPARK: light-gated K^+ channels

SPARK (Synthetic Photoisomerizable Azobenzene-Regulated K^+ channel) was the first genetically-targeted PTL-based system invented and the first optogenetic system for silencing neuronal activity [53]. In this system the PTL consists of a *M*aleimide (the cysteine-reactive group), an *A*zobenzene, and *Q*uaternary ammonium (a K^+ channel pore blocker) (MAQ). Once attached to the *Drosophila* Shaker K^+ channel at an introduced cysteine residue, conduction through the channel is blocked by 500 nm light and unblocked at 380 nm. The relatively large (about 20 pS) conductance of the Shaker K^+ channel [54], combined with robust expression in mammalian neurons, makes this an effective tool for optically inhibiting action potential firing [7,53].

Subsequently, SPARK was modified to function as a trigger for optically depolarizing neurons and inducing action potential firing [55], since it was seen that a single point mutation in the ion selectivity filter could significantly increase its permeability to Na^+ [56]. This modified version is called D-SPARK (D stands for "depolarizing"), and triggers action potentials when the pore is unblocked by 380 nm illumination by allowing Na^+ conduction into neurons. These action potentials cease upon 500 nm illumination.

Since both SPARK and D-SPARK bind the same PTL, the two channels could be genetically targeted to different populations of neurons, which would then be endowed with light sensitivity upon binding of MAQ.

LiGluR: Light-Gated Kainate-Type Glutamate Receptor

The success of azobenzene-tethered ligands and their utility in complex cellular systems encouraged Trauner, Kramer, and Isacoff to extend this concept to other important ion channels [3]. Specifically, ionotropic glutamate receptors (iGluRs), which are the major mediators of excitatory synaptic transmission in the central nervous system [57], proved ideal candidates because of their well characterized pharmacology and the availability of 3D structural data [58].

iGluRs are a family of ligand-gated cation channels, which according to their pharmacological profile are categorized as receptors for:

- AMPA (GluA1-4)

- Kainate (GluK1-5)
- NMDA (GluN1, GluN2A-D, GluN3A-B)

In vivo, these receptors can either be homo- o hetero- tetramers. Each of the four subunits is characterized by three domains: a transmembrane pore-forming domain (TMD), an extracellular ligand-binding domain (LBD), and an N-terminal domain (NTD) responsible for controlling the subunit oligomerization. The reversible binding of the ligand and, consequent closure of the clamshell-like LBD, is directly coupled with the opening of the pore [59] (Figure 3).

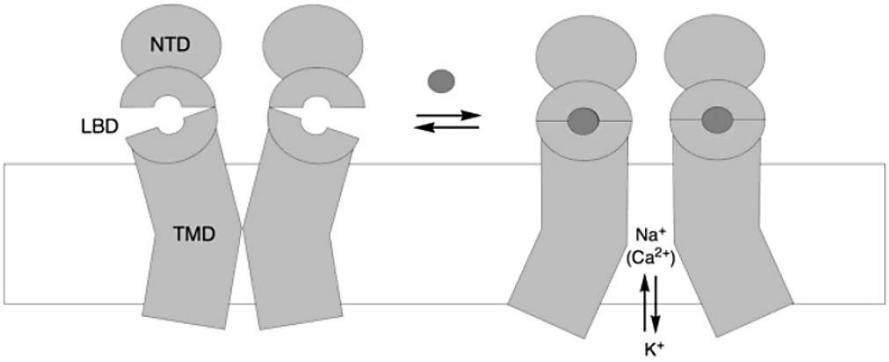

Figure 3: Schematic representation of the native function of iGluRs. (from Banghart et al. 2006 [58])

The availability of the structural 3D data of iGluRs lays the groundwork both for understanding their pharmacology and for their re-engineering.
It was revealed by the crystal structure of iGluK2 bound with the agonist (2S,4R)-4-methyl glutamate that the ligand-bound form of the clamshell, although closed, features a narrow "exit tunnel" connecting the binding pocket to the extracellular surface [60]. The idea was that this tunnel could enable a tether appended to an agonist to protrude and reach an attachment site at the surface of the protein, while permitting the clamshell to close over the agonist and activate the channel [3]. A glutamate analogue could be threaded through the tunnel and attached to an appropriately positioned mutant cysteine residue, on the exterior of the LBD, via a photoswitchable tether, providing the basis for a light activated iGluR. Once attached, the glutamate would activate the channel every time the photoswitch would change its conformation to its *cis* form, inserting the agonist in the LBD (Figure 4).

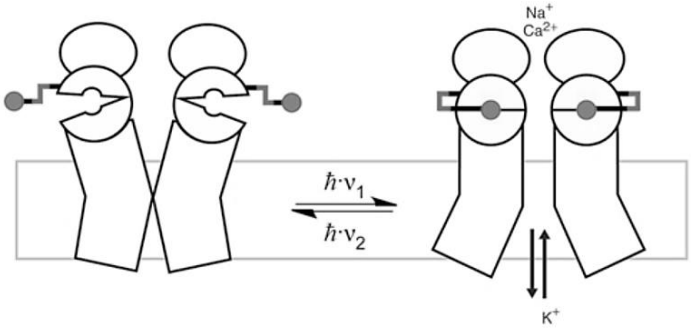

Figure 4: Design of a light-gated iGluR (LiGluR). On the left we can see the PTL in its *trans* configuration bound on the LBD. After exposure to an adequate wavelength, the photoisomerizable linker bends: the molecule of glutamate is led into the LBD and the channel is opened (image from Reiner & Isacoff, 2014 [10]).

The PTL designed for these receptors is called MAG, and is formed by a *M*aleimide, an *A*zobenzene, and a molecule of *G*lutamate (Figure 5). The maleimide is the reactive group which binds to the receptor in proximity of the LBD. Bound to the maleimide is the photoisomerizable linker azobenzene. The activation of the channel occurs due to a molecule of glutamate bound to one end of the azobenzene linker, so when the linker "bends" the glutamate fits into the LBD.

cis-MAG was shown to covalently bind to an iGluK2 mutant that possessed a cysteine substitution at amino acid position 439 (L439C), with persistent channel activation. Subsequent isomerization to the *trans* form of the azobenzene led to a significant reduction in current [3]. This mutant was the one that showed the greatest response across a series of iGluK2 cysteine mutants. Site directed mutagenesis was performed on amino acid that formed a perimeter around the exit tunnel, close to where the maleimide end of the tether was predicted to stick out. Ca^{2+} imaging was used to test cysteine mutants, to see which one would provide optical activation after covalent attachment of MAG. This assay allowed to rapidly test 11 positions and find 3 with clear responses to light, in which calcium concentration increased at 380 nm and declined back to basal levels at 500 nm. Of the 3, iGluK2-L439C had the largest response.

To better characterize the kinetics of channel gating and to obtain quantitative measures of activation efficiency, whole-cell patch clamping was performed.

These experiments showed that iGluK2-L439C conjugated with MAG (LiGluK2) was activated both by free glutamate and by illumination. By means of different steps of illumination it was possible to determine the two peaks for photoisomerization: 380nm for the *cis* form, 500 nm for the trans form. In addition to this, it was shown that repeated switching between 380 and 500 nm evoked responses of similar amplitude over a period of more than 30 minutes, which is consistent with the resistance of azobenzenes to bleaching, demonstrating that the system is robust. It was also observed that even with weak illumination from a standard fluorescent lamp, attenuated by passage through a monochromator and fiber guide, the receptor turned on and off rapidly (τon-380 nm = 115 ± 3 ms and τoff-500 nm = 92.3 ± 0.3 ms; mean ± s.e.m., n = 3) at a power of 12.4 W m^{-2} (irradiance at 500 nm) [3].

The responses obtained via illumination were smaller than those generated by saturating concentrations of glutamate (300 µM). Initially it was thought that this could be due to incomplete labelling, but increased exposure to MAG (in either concentration or time) during the conjugation period did not change the size of the optical response. The alternative explanation is that MAG allows an incomplete closure of the LBD, which has been previously linked to partial agonism in the related iGluA2 channel [61].

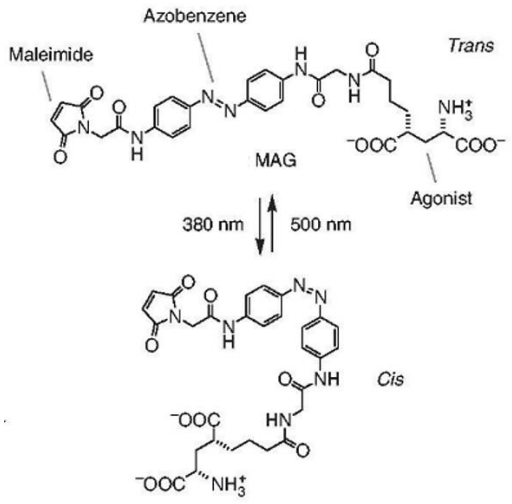

Figure 5. MAG and its two isomers. In this case, 380 nm light causes the azobenzene linker to bend into its *cis* isomer, while 500 nm light leads the molecule back to its *trans* configuration (image from Volgraf et al, 2006 [3])

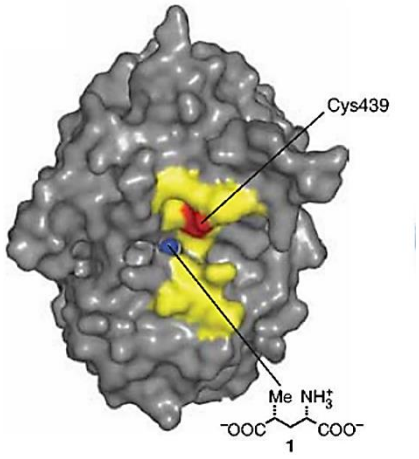

Figure 6: Mutations in the GluK2 LBD. Residues that were individually mutated to cysteine are shown in yellow; cysteine 439 is shown in red; in blue, the methyl group of (2S,4R)-4-methyl glutamate (1), at the bottom of the exit tunnel (image from Volgraf et al. 2006 [3]) .

MAG ligands with different linker lengths and stereochemistry have been developed [51], and those that work well in combination with LiGluK2 are L-MAG0 and L-MAG1[10]. Under physiological ionic conditions, activation of the receptor leads to a net influx of positive ions, mostly Na^+[62]. The Ca^{2+} and Cl^- permeability of GluK2 is largely controlled by the Q/R editing site located in the pore loop [63]. The fast kinetics of iGluK2 (τ_{on} = 0.12-0.22 ms [64]) and its single channel conductance is (25 pS for homomeric iGluR6Q [65]) make it a particularly suitable candidate for rapid, robust optical control of neural activity.
Apart from its optical controllability, LiGluR resembles native GluK2 receptors in all key aspects, displaying normal glutamate affinity [66] as well as normal desensitization and recovery properties [67]. In addition to this, LiGluR expression and labelling was shown to not alter cell health [68] or the number of presynaptic inputs [69].
GluK2 (formerly GluR6) plays distinct roles at excitatory and inhibitory synapses throughout the brain and has been implicated in a variety of neurological diseases, including mood disorders and epilepsy [1,2]. The conservation of native GluK2 properties provides an opportunity to further engineer LiGluR based on known principles of receptor function in order to make designer variants for specific applications [52].

Numano *et al.* [70] subsequently created converse light sensitivity in the LiGluR system, termed *trans*-LiGluR, so that the receptor is activated by 500 nm light and deactivated by 380 nm light. This was achieved by shortening the length of MAG and relocating the anchoring cysteine residue (G486C). This means that the GluK2 mutants can be genetically targeted to different populations of neurons and then treated with the same PTL, allowing activity to be triggered in one group of cells by 380 nm light and in another group of cells by 500 nm light [7].

In 2010, Janovjak *et al*. [71] furtherly modified the LiGluR system. Chimeras were constructed in which the transmembrane helices and re-entrant pore-loop of the K^+-selective sGluR0 were transplanted into iGluK2, and the best of these was modified for light-gating and termed HyLighter, which can be used to hyperpolarize neurons.

LiGluRs have been used for studies in a variety of neurobiological model systems, such as primary neurons [90,91], astrocytes [92], neuroendocrine cells [93], in the mouse retina [94], the fly neuromuscular junction [95], and zebrafish [90,96,97].

In the last couple of years, LiGluK2 has been further engineered, as reported in the work of Levitz *et al*. in 2016 [52], where LiGluR responses were tuned with MAG variants, and for the first time the use of this optical tool was established *in vivo* in mice. The main difference is the use of a single-wavelength MAG, MAG_{460} [72]. This PTL shifts to its *cis* form with an illumination of 440-480 nm (blue light) but has a fast thermal relaxation which allows it to quickly go back to the *trans* form in the dark (τ_{mean} = 0.71 s). L-$MAG0_{460}$ photoswitches offer the simplicity of one color photocontrol, and intensity-dependence of L-$MAG0_{460}$ allows for photoswitching effects to be titrated by adjusting the laser intensity. In addition to this, MAG_{460} photoswitches, unlike regular MAGs, may also be activated via two-photon infrared light illumination, which provides high spatial precision and enhanced tissue penetration [73,74]. What the authors sustain is that both dual-color "regular" MAG photoswitches and single-color MAG_{460} photoswitches may be employed in cultured neurons and *in vivo* with comparable efficacy. These two families of photoswitches provide distinct advantages that allow for appropriate adaptation to the given application. In the study of Levitz *et al*., LiGluR was used *in vivo* in the neocortex of adult mice in conjunction with fiber-based optogenetic technologies, allowing rapid optical control of GluK2 activity. AAV-mediated expression of LiGluR in visual cortex was found to

produce enough levels of surface GluK2 in cortical neurons after ~3 weeks. MAG labeling was shown to occur rapidly following injection and showed no obvious adverse effects neither on animal nor on tissue health. Moreover, they demonstrated that it permits selective photoactivation of engineered receptors within a pool of native receptors and that it remains bound to LiGluRs for at least 24 hours post-labeling, greatly expanding the applicability of MAG photoswitches to control LiGluRs. In the neocortex, LiGluR photoactivation was found to induce more than a 10-fold increase in firing rate with rapid onset and offset (as fast as ~30ms; average ~100ms). Photoswitching was highly reversible and repeatable over many trials, and was seen throughout all layers of the cortex, indicating that this approach can likely work throughout all regions of the mammalian brain where optical fibers can be implanted. Photoactivation modulated the activity of both low-firing and fast-firing neurons, so, considering the ability to manipulate a high percentage (60%) of cells within a given cortical region, LiGluR- mediated photoactivation is likely robust enough for behavioral manipulations as well as cell-type-specific interrogation of neuronal circuits. The success of LiGluR *in vivo* will pave the way for further application of PTL-based tools to probe specific proteins in circuit function and higher-level brain activity.
One of the key features of the PTL-based approach is that the protein of interest may be genetically modified but maintaining the possibility of specific manipulation through photoswitch conjugation. This means that we can introduce mutations in regulatory of functional sites within LiGluR without altering its ability to become photo-activated by MAG, in order to directly test the role of the mutated residues in receptor function. This is a great improvement over classical knock-in approaches in terms of both spatial and temporal control.
In addition to this variant of the LiGluK2-MAG_{460} system, the study of Levitz *et al.* shows three variations of LiGluK2. One of the variants, termed LiGluR(R), shows a decreased Ca^{2+} permeability due to the mutation of a single key residue in the pore region. Using this modified receptor in neurons will allow to test the importance of calcium influx, as opposed to membrane depolarization alone, in mediating the physiological downstream effects of GluK2. This approach may be also applied to other residues, in order to create variants that have altered activation and desensitization kinetics, phosphorylation sites, or other key properties of kainate receptors.

Similarly, they also engineered LiGluR to have a lower affinity for glutamate. This was done with the idea of a receptor that is activated only by light, to better understand the role of LiGluR against the background of normal glutamatergic transmission. Additional mutations were done in order to lower the receptor's affinity to glutamate, maintaining, however, a robust expression and high enough affinity to respond to MAG. Two variants were created: LA-LiGluR and ULA-LiGluR. LA-LiGluR (Low Affinity LiGluR) presents a K487A substitution in addition to L439C, and a reduced sensitivity to glutamate (EC50∼ 0.70mM) while MAG photoswitching is retained. ULA-LiGluR, on the other hand, is the "Ultra Low Affinity" variant which has a strongly reduced affinity for glutamate (EC50∼ 10mM) while L-MAG1 photoswitching is retained.

Together, these variants constitute a LiGluR toolset that may be further enhanced by combination of GluK2 mutants with different versions of L-MAG. A summary of MAG photoswitches and LiGluR variants are shown in Table 1.

Even though the labeling of the receptors with a PTL has to be optimized for each preparation and controls on specificity have to be included, this approach offers many advantages compared to the opsin-based approach. It allows to toggle signaling proteins which are native to the synapse and control more specific functions compared to simply varying the membrane potential.

Compared to classical optogenetic approaches this PTL-based strategy does not only allow to control cellular excitability, but to probe the function of specific receptor subtypes and their contribution to behavior with unprecedented resolution [52]. In addition to this, the reasons we decided to use this approach over classic optogenetics, is that it can overcome one of the obstacles in the use of ChRs: channel conductance. Conductance directly determines the effectiveness of light-induced depolarization [75]. The estimation of single channel conductance of ChR2 is below 1 pS [76], which is less than the conductance of the common membrane channels and much lower than the 25 pS conductance of the homomeric GluK2 receptor. In addition to this, as mentioned above, LiGluK2 maintains all the key features of native GluK2 receptors.

A. MAG Photoswitch

Name	Photoswitching	Key features	References
L-MAG0 L-MAG1 L-MAG2	*cis*: 370–395 nm *trans:* 460–540 nm	Series of bistable photoswitches with different linker lengths that turn LiGluRs *on* and *off* with light of different wavelengths; thermal relaxation occurs on slow timescales (τ = 26 min) rendering switching bistable	Numano et al., 2009
L-MAG0$_{460}$	*cis*: 440–480 nm *trans:* darkness	Single-wavelength photoswitch (blue-light activated) with fast thermal relaxation (τ_{mean} = 0.71 s); also activated by white light and 2-photons (850 nm)	Kienzler et al., 2013; Izquierdo-Serra et al., 2014; Carroll et al., 2015
toCl-MAG1	*cis*: ~ 380 nm, >540 nm *trans:* ~ 440 nm	Activated with UV, yellow and red light (but slower kinetics at comparable light intensities); bistability through slow thermal relaxation (τ = 5 h)	Rullo et al., 2014

B. Engineered Receptor

Name	Mutations	Key features	References
LiGluR	L439C	General light activated glutamate receptor based on GluK2(Q)*; *cis*-MAGs cause receptor activation, which results in depolarization	Volgraf et al., 2006; Gorostiza et al., 2007
LA-LiGluR	L439C K487A	Reduced sensitivity to glutamate (EC_{50}~ 0.70 mM) while MAG photoswitching is retained	This study
ULA-LiGluR	L439C E738D	Strongly reduced sensitivity to glutamate (EC_{50}~ 10 mM) while L-MAG1 photoswitching is retained	This study
LiGluR(R)	L439C Q621R	Low Ca^{2+} permeability (Q/R editing site in GluK2)	This study
trans-LiGluR	G486C	Reversed mode of action (*trans*-activated with L-MAG0)	Numano et al., 2009
Hylighter	P0-C chimera L439C	K^+-selective LiGluR for hyperpolarization/silencing	Janovjak et al., 2010

Versatile LiGluR toolset provided by combining (A) different MAG photoswitches with (B) engineered receptors variants.
** standard LiGluR is based on the GluK2a isoform with Q621 (unedited).*

Table 1 Available MAG photoswitches and LiGluR variants (Table from Levitz et al. 2016 [52]).

THE ROLE OF CALCIUM IN NEURONS AND CALCIUM IMAGING

A great variety of calcium signals is used by virtually every cell type in biological organisms, including the control of heart muscle contraction [77] and the regulation of vital aspects of the entire cell cycle, from cell proliferation to cell death [78,79]. The characteristics of these signals depend on the expression of tissue-specific calcium transport systems [80]. The diversity of cellular calcium signalling means that there is no single technique that can be used to monitor calcium changes in all situations. However, fluorescent calcium indicators and imaging provide the most versatile and widely used method for analysing cellular calcium responses. Using appropriate technology and suitable indicators, it is possible to monitor Ca^{2+} signals spanning from subcellular to multicellular, at high speed or time lapse, within living cells [81].

Calcium in Neurons

In the nervous system, calcium has a plethora of functions, also due to the complex morphology of neurons [82]. At the presynaptic terminal, calcium influx triggers the exocytosis of the synaptic vesicles which contain neurotransmitters[83]. Postsynaptically, a transient rise of the calcium level in dendritic spines is essential for the induction of activity-dependent synaptic plasticity [84]. In the nucleus, calcium signals can regulate gene transcription [85]. All these processes regulated by intracellular calcium present a wide variability in terms of time range, since neurotransmitter release occurs at the microsecond scale, while gene transcription lasts from minutes to hours [86]. This means that the time course, the amplitude, the localized action in well-defined cellular subcompartments are essential determinants for the function of intracellular calcium signals [82].

Only free calcium ions are biologically active, so the maintenance of a low intracellular calcium concentration when the neuron is at rest is fundamental. At rest, most neurons have an intracellular calcium concentration that ranges between 50 and 100 μM, which can transiently rise during electrical activity to levels that can be from 10 to 100 times higher [80]. Speed and effectiveness of calcium are due to the gradient maintained by cells between their intracellular and extracellular concentrations. Cells invest much of their energy to effect changes in calcium concentration, and since calcium cannot be chemically altered, cells must chelate, compartmentalize, or extrude calcium in order to control its concentration [87]. Cytosolic calcium concentration is determined both by the balance between influx and efflux of calcium ions, and the exchange of calcium from internal stores [82]. Multiple different mechanisms are responsible for the calcium influx from the extracellular space, including voltage-gated calcium channels, ionotropic glutamate receptors, nicotinic acetylcholine receptors (nAChR), and transient receptor potential type C (TRPC) channels [88–90]. On the other hand, calcium efflux, namely the removal of calcium from the cytosol, is performed by the plasma membrane calcium ATPase (PMCA), the sodium-calcium exchanger (NCX), and the sarco-/endoplasmic reticulum ATPase (SERCA) [86]. As for the internal calcium stores, these are mainly the endoplasmic reticulum (ER) and the mitochondria, which are both important for neuronal calcium homeostasis. The high level of calcium inside the ER is maintained by the SERCA that transport calcium ions from the cytosol to the lumen of the ER. Mitochondria,

on the other hand, can act as calcium buffers by taking it up through the calcium uniporter during cytosolic calcium elevations and then releasing it slowly through sodium-calcium exchange [91]. Calcium release from the internal stores, mostly the ER, is mediated by inositol triphosphate receptors (InsP3R), which can be produced by metabotropic glutamate receptors, and ryanodine receptors (RyRs) [92].

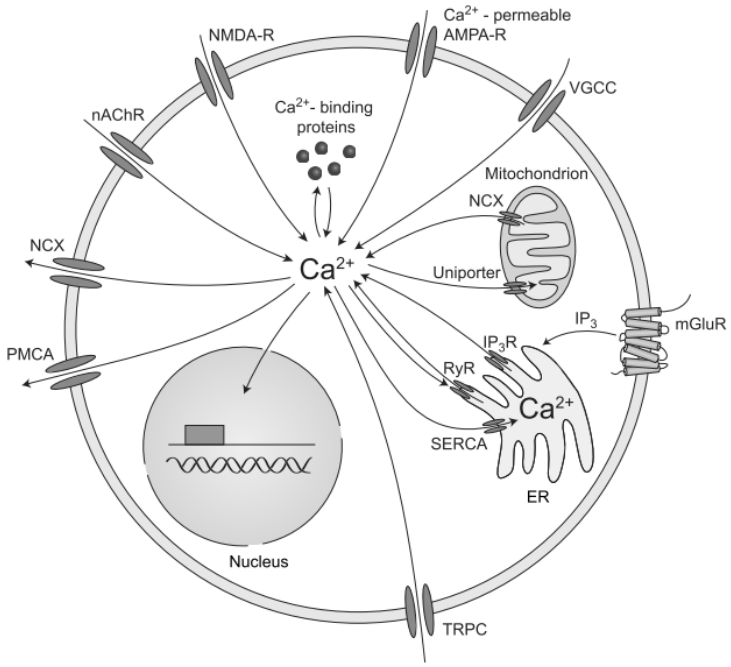

Figure 7: Calcium in neurons (Image from Grienberger &Konnerth, 2012 [82])

Imaging Calcium in Neurons

A wide variety of calcium indicators is available, with excitation and emission spectra ranging from ultraviolet (UV) to the far red, and with different cell permeability, basal fluorescence and Ca^{2+} affinity. The choice of the calcium indicator must be evaluated considering two main factors: the calcium signal to be measured and the importance of quantitative or qualitative data.

Calcium indicators can be distinguished in two main categories:

- Chemical calcium indicators
- Genetically Encoded Calcium Indicators (GECI)

Chemical Calcium Indicators

Chemical calcium indicators are widely used for the investigation of intracellular Ca^{2+} signalling. Chemical calcium indicators derive from the combination of a chelator and a fluorophore (Figure 8). The binding of calcium ions causes intramolecular conformational changes that lead to a change in the emitted fluorescence.

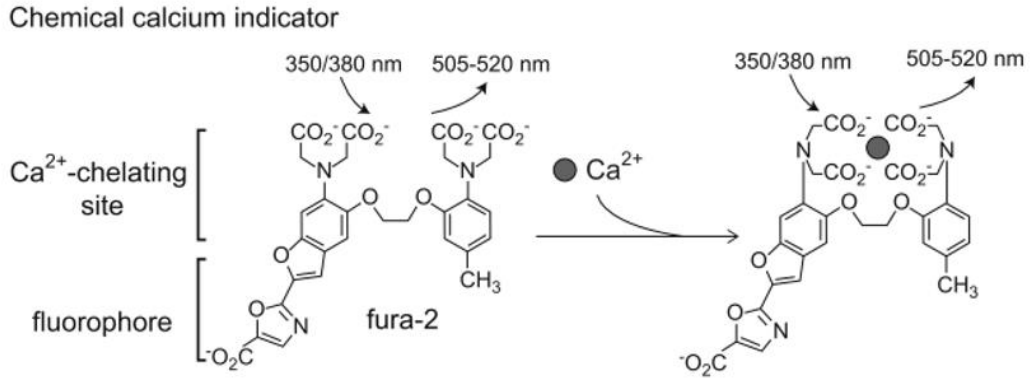

Figure 8: Example of chemical calcium indicator Fura-2. Upon Ca^{2+} binding intramolecular conformational changes cause a change in emitted fluorescence. (Image from Grienberger &Konnerth, 2012 [82])

Calcium indicator dyes are commercially available in three chemical forms, indicators of their membrane permeability:

1. Salts
2. Dextran conjugates
3. Acetoxymethyl (AM) esters.

1. Salts

Salts are the simplest form of calcium indicators but are membrane impermeable. This means that they require invasive loading procedures such as: diffusion via patch-clamp pipette, microinjection, electroporation and lipotransfer using liposomes. Once loaded, the cells are ready for imaging within minutes. The drawback of this kind of indicator is that it tends to be compartmentalized into membrane bound vacuoles. This degrades calcium

measurements within the cytosol, but is not a major problem in short recordings (30-60 min) [93].

2. **Dextran Conjugates**

   To address the problem of compartmentalization, dextran conjugates were developed. These conjugates present high water solubility, low toxicity, and exhibit essentially no compartmentalization over very long recording periods up to days in length, but, like salts, they are membrane impermeable and require invasive loading.

3. **Acetoxymethyl (AM) esters**

   Calcium indicator dyes engineered with AM esters offer a more convenient method for loading hydrophilic dyes into cells. Acetoxymethil (AM) esterification makes the dyes membrane permeable: they enter and remain inside of the cell after intracellular esterases cleave the AM group. This allows us to passively load the dye inside the cells by adding it to the extracellular medium.

Chemical calcium indicators also present different calcium affinity. The most used are high affinity calcium dyes, which are well characterized and come in an array of spectral properties and binding affinities that can be utilized to suit the needs of most experiments. Low affinity calcium dyes, instead, are used when very little buffering is tolerated or in subcellular compartments, where calcium concentration is much higher.

In addition to these factors, the Ca^{2+} dependent spectral changes that occur must also be carefully considered. Indicators can be classified as single- or dual-wavelength, which are used for qualitative and quantitative measures respectively. Both classes require specific lasers, filters, and/or detection methods that are dependent upon their spectral properties and both classes have advantages and limitations. Single-wavelength calcium indicators are generally very bright and optimal for imaging together with other fluorophores. They exhibit significant Ca^{2+} dependent changes in fluorescence intensity without shifting their excitation or emission wavelengths. It is easier to avoid or minimize spectral overlap with other fluorophores when working with single-wavelength indicators [94–96].

Dual-wavelength, or ratiometric, indicators shift the peak wavelength of either their excitation or emission curve upon binding Ca^{2+} an thus can be precisely calibrated. In addition to this they minimize the most common problems associated with chemical indicators, including uneven dye loading, leakage, photobleaching and changes in cell volume, but at the cost of increased spectral bandwidth. In Table 2 general characteristics of some available dyes are presented.

High affinity calcium indicators.

Indicator	K_d for Ca^{2+} (nM)	Excitation (nm), emission (nm)	Notes
Calcium Green-1	190	490 ex, 531 em	Single wavelength
Fluo-3	325	506 ex, 526 em	Single wavelength
Fluo-4	345	494 ex, 516 em	Single wavelength
Fura-2	145	363/335 ex, 512 em	Dual excitation/single emission
Indo-1	230	488 ex, 405/485 em	Single excitation/dual emission
Oregon Green 488 Bapta-1	170	488 ex, 520 em	Single long wavelength
Fura-4F	0.77	336/366 ex, 511 em	Ratiometric excitation/single emission
Fura-5F	0.40	336/363 ex, 512 em	Ratiometric excitation/single emission
Calcium Crimson	185	590 ex, 615 em	Single long wavelength
X-Rhod-1	0.7	580 ex,602 em	Single excitation/emission

Low Affinity Ca^{2+} indicators.

Indicator	K_d for Mg^{2+} (mM)	K_d for Ca^{2+} (μM)	Excitation (nm), emission (nm)	Notes
Mag-Fura-2	1.9	25	329/369 ex, 511em	Ratiometric excitation/single emission
Mag-Fluo-4	4.7	22	490 ex, 517 em	Single excitation/emission
Mag-Indo-1	2.7	35	349 ex, 480/390 em	Single excitation/ratiometric emission
Mag-Fura-5	2.3	28	369 ex, 505 em	Ratiometric excitation/single emission
Mag-Fura-Red	2.5	17	488 ex, 630 em	Ratiometric excitation/single emission
Fura-2-ff	–	35	335/360 ex, 505 em	Ratiometric excitation/single emission
Fluo-5 N	–	90	491 ex, 516 em	Single excitation/emission
Oregon Green BAPTA-5N	–	20	494 ex, 521 em	Single excitation/emission
Fura-6F	–	5.3	336/364 ex, 512em	Ratiometric excitation/single emission
Fura-FF	–	5.5	335/364 ex, 510em	Ratiometric excitation/single emission
Fluo 5 F	–	2.3	491 ex, 518 em	Single excitation/emission
Fluo 4FF	–	9.7	491 ex, 516 em	Single excitation/emission
Oregon Green 488 BAPTA-6F	–	3	494 ex, 524 em	Single excitation/emission
Rhod-FF	–	19	552 ex, 580 em	Single excitation/emission
X-Rhod-5F	–	1.6	581 ex, 603 em	Single excitation/emission
X-Rhod-FF	–	17	580 ex, 603 em	Single excitation/emission

Table 2 Characteristics of high and low affinity calcium indicators (Table from Paredes et a., 2008 [97])

Genetically Encoded Calcium Indicators (GECI)

GECIs, unlike chemical calcium indicators, allow recordings from molecularly defined cell types or even subcellular compartments. They do not need to be loaded into cells, and the genes encoding for these proteins can be easily transfected in cell lines. It is also possible to create transgenic animals expressing the dye in all cells or selectively in certain cellular subtypes. This is made possible by their conjunction with cell specific promoters [98], targeting sequences [99,100], and the use of the Cre-loxP system [101].

GECIs can be categorized in two classes, defined by the number of fluorophores present in the indicator:

- Single-fluorophore GECIs (one fluorescent protein)
- FRET-based GECIs (two fluorescent proteins)

These indicators are fluorescent proteins derived from green fluorescent protein (GFP) or its variants (e.g. circularly permuted GFP, YFP, CFP), fused with calmodulin (CaM) and the M13 domain of the myosin light chain kinase, which is able to bind CaM. Alternatively, two fluorophores, variants of GFP, are used and the mechanism of FRET (Förster Resonance Energy Transfer) for signal modulation is applied (Figure 9).

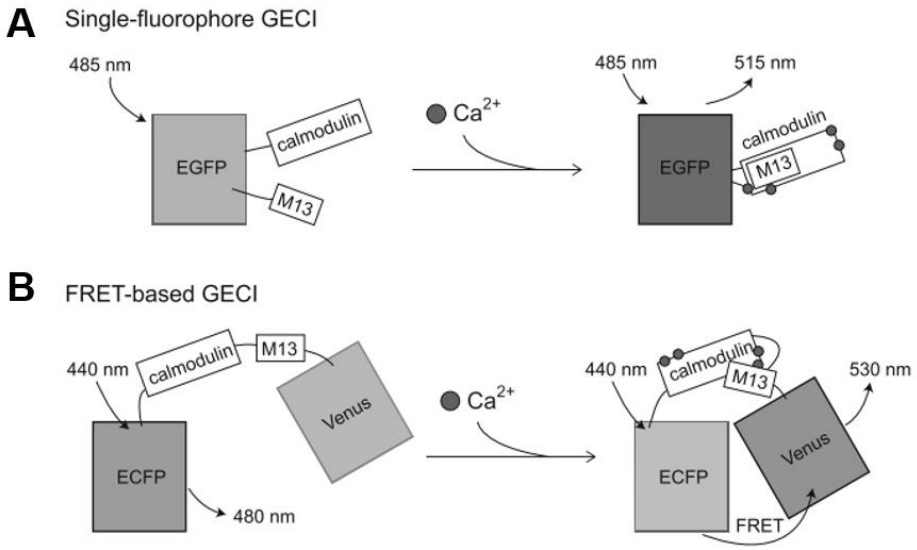

Figure 9: Genetically Encoded Calcium indicators. A. Single-fluorophore GECI of the GCaMP family; calcium binding causes interaction between CaM and M13, leading to a change in the conformation of the fluorophore EGFP and a consequent increase of fluorescence emission. **B.** FRET-based GECI contain two fluorophores. Here depicted is YC 3.60 of the cameleon family, which contains the fluorescent proteins ECFP (blue) and Venus (yellow). In absence of calcium, the predominant fluorescence is blue, but calcium binding CaM leads to a shortening of the distance between ECFP and Venus allowing FRET to occur: Venus is excited and emits photons, leading to an increase in yellow fluorescence.

Single-Fluorophore GECIs

Single-fluorophore GECIs (Figure 9A) share a common principle of action that involves a change in for their fluorescence intensity upon Ca^{2+} binding. In most available indicators, Ca^{2+}-chelating properties are provided by the calmodulin moiety, fused to the fluorescent protein and to the calmodulin-binding peptide M13. The binding of Ca^{2+} causes an intramolecular rearrangement that alters the fluorophores protonation state and its associated fluorescent properties [102,103]. Since the chromophore chemical structure is not modified during conformational rearrangement, the change in fluorescence is associated with an increase or decrease in the absorption spectra, which leads to a change in the intensity of the emitted fluorescence. Because only a single-wavelength is measured, these types of indicators are known as intensiometric or non-ratiometric [104]. An example of these GECIs is GCaMP, depicted in Figure 9A. GCaMPs consist in a circularly permuted EGFP, flanked on one side by the calcium-binding protein calmodulin (CaM) and the CaM-binding peptide M13 on the other [105]. In. The presence of calcium causes the interaction between CaM and M13, leading to conformational changes in the fluorophore's environment that cause an increase in the emitted fluorescence [26,105].

FRET-based GECIs

Calcium imaging using GECIs containing two fluorophores is based on the concept of Förster Resonance Energy Transfer (FRET). During FRET, one of the fluorescent proteins acts as a donor that, when excited, transfers absorbed energy to the second fluorescent protein, the acceptor. The efficiency of this energy transfer is highly dependent on the distance between the donor and the acceptor moieties [106], which must be less than 10 nm. GECIs are designed in such a way that after Ca^{2+} binding the FRET efficiency increases, either due to closening of the two fluorescent protein moieties or due to changes in their relative orientations. The efficiency of FRET also depends on several other factors, such as the overlapping of donor emission and acceptor absorption spectra, donor lifetime, and relative orientation of the donor and acceptor transition

dipole moments [106]. The example in Figure 9B shows the FRET-based GECI yellow cameleon 3.60 (YC 3.60). It is composed of the Enhanced Cyan Fluorescent Protein (ECFP) and the circularly permuted Venus, the donor and the acceptor respectively. The linker sequence that connects these two proteins is formed by the CaM and the peptide M13 [107]. In the absence of calcium ions, the emission is dominated by the blue ECFP fluorescence (480 nm). When calcium binds to CaM, intramolecular changes lead to a shortening of the distance between ECFP and Venus. Because of this, Venus is excited due to the FRET and emits photons of about 530 nm, leading to a reduction of the blue fluorescence and an increase of the yellow fluorescence. The calcium signal is expressed as a ratio between the two.

A major advantage chemical calcium indicators over GECI is the broad range of indicators with different calcium affinity commercially available in addition to the ease of introducing and rapidly using these dyes for experiments [93]. A major disadvantage, on the other hand, is that, unlike GECI, they cannot be specifically targeted to a certain cell-type or organelle. Chemical indicators also tend to compartmentalize and are eventually extruded over long recording experiments [108,109], while GECI allow for chronic recordings over several days, since they are functional in neurons over long periods of time [26,110,111].

Imaging equipment and readout

Regardless of the type of indicator used, the imaging procedure is generally quite similar. Cultured cells loaded with an indicator, or expressing it in the case of GECI, can be viewed using a fluorescence microscope and captured by a CMOS or CCD camera. Imaging calcium in neurons at deeper locations in the brain or spinal cord is usually performed by using confocal or two-photon microscopy [82]. Confocal and two-photon microscopes provide improved sectioning ability so that calcium signals can be resolved in micro domains.

For single wavelength excitation/emission dyes, the simplest procedure is to divide changes in the fluorescent signal by the average resting fluorescence according to the formula [97]:

$$\Delta \mathrm{Ca}^{2+} = \frac{\Delta F}{F} = \frac{F - \mathrm{F_{rest}}}{\mathrm{F_{rest}}}$$

For dual-wavelength dyes, on the other hand, images are analysed by measuring fluorescence intensity changes of two wavelengths expressed as a ratio (ratiometric indicators). The derived fluorescence intensities and ratios are plotted against calibrated values for known Ca^{2+} levels to learn Ca^{2+} concentration.

MATERIALS & METHODS

CELL CULTURE

Hippocampal neurons from Wistar rats (P2-P3) were prepared in accordance with the guidelines of the Italian Animal Welfare Act, and their use was approved by the Local Veterinary Service, the SISSA Ethics Committee board and the National Ministry of Health (Permit Number: 630-III/14) in accordance with the European Union guidelines for animal care (d.1.116/92; 86/609/C.E.). The animals were anaesthetized with CO2 and sacrificed by decapitation, and all efforts were made to minimize suffering. Glass coverslips (18 mm diameter) were coated with 50 μg/ml poly-l-ornithine (Sigma-Aldrich, St. Louis, MO, USA) overnight, and a thin layer of Matrigel® (diluted 1:50 with culture medium; Corning, Tewksbury MA, USA) was applied just before cell seeding. Dissociated cells were resuspended in Neuronal medium with the following composition: minimum essential medium (MEM) with GlutaMAX™ supplemented with 10% dialyzed fetal bovine serum (FBS), (all from Thermo Fisher Scientific, Waltham, MA, USA), 0.6% D-glucose, 15 mM HEPES, 0.1 mg/ml apo-transferrin, 30 μg/ml insulin, 0.1 μg/ml D-biotin, 1 μM vitamin B12 and 2.5 μg/ml gentamicin (all from Sigma-Aldrich). Cells were plated at a density of 90’000 cells per coverslip and incubated for 30 min at 37 °C. For each coverslip, placed in a 12-well tissue culture plate, 2 ml of culture medium were then added. Half of the medium was changed after 24 h and 2 μM cytosine-β-D-arabinofuranoside (Ara-C; Sigma-Aldrich) was added to all culture media in a 1:1000 proportion. The concentration of FBS (in medium containing 10% FBS) was decreased to 5%. The neuronal cultures were maintained in an incubator at 37 °C, 5% CO2 and 95%

relative humidity. Medium was not changed again, fresh medium was added at the moment of transfection only, according to protocol.

TRANSFECTION

The plasmid used was genetically-targeted to neurons by means of the Human Synapsin 1 (hsyn1) promoter. The LiGluK2-GFP DNA was kindly provided by Professor E.Y. Isacoff. At DIV7 cells were transfected with 1µg/µl LiGluK2 (Effectene Transfection Kit, Qiagen). After 48 h, cells reached maximum expression and were ready for calcium imaging. GFP reporter expression allowed us to identify transfected neurons.

CALCIUM IMAGING AND RHOD-3 AM

Rhod-3 AM (Rhod-3 AM Calcium Imaging Kit, Life Technologies) is a calcium dye designed for live-cell imaging of cytosolic calcium signaling in combination with green-fluorescent dyes or proteins. Compared to existing red calcium dyes, Rhod-3 AM exhibits a large increase (>2.5 fold) in fluorescence upon binding Ca^{2+} and very low fluorescence at rest (without Ca^{2+} binding). Moreover, it displays a more uniform cytosolic distribution and improved signal compared to existing red calcium dyes such as Rhod-2.

Rhod-3 AM has particular spectral properties: its peak excitation is around 560 nm, while its emission is around 600 nm. Consequently, the excitation and emission peaks are very close to one another (Figure 10). Narrow emission enables simultaneous detection with GFP or other dyes. In our experiments, the closeness of the two peaks allows to intertwine various wavelengths reducing overlapping to a minimum (Figure 11). In addition to GFP excitation, we had to consider the activation and inactivation wavelengths of LiGluK2, 370-390 nm and 480-530 respectively.

At 48h from transfection, cells were prepared for Ca^{2+} imaging. Ringer solution was used for the recordings (145 mM NaCl, 3 mM KCl, 1.5 mM $CaCl_2$, 1 mM $MgCl_2$, 10 mM glucose and 10 mM HEPES, pH 7.4). At room temperature, cells were first incubated 30 minutes in a Loading Buffer (2ml Ringer, 20µl PowerLoad, 20µl Probenecid, 2µl Rhod-3 AM), then 30 minutes in an Incubation Buffer (2ml Ringer, 20 µl Probenecid). After this, cells were incubated at 37 °C with L-MAG0 (kindly provided by Professor Isacoff, and A. Barberis' laboratory [IIT]) for 30 minutes. L-MAG0 was diluted in Ringer solution immediately prior to incubation in order to reach a 10 µM final concentration. The coverslip with the hippocampal culture was fixed in a low profile open bath chamber (RC-

41LP, Warner Instruments) and Ringer solution was added. The chamber was then placed over the 20x microscope objective. Once the transfected neurons were localized by GFP expression, we proceeded with Ca^{2+} imaging. Recordings were performed with a digital CMOS Hamamatsu Orca Flash 4.0 camera, connected to a 4x magnification tube, reaching an 80x total magnification. The software used during recordings was HCImage Live, and the duration varied from 5 to 10 minutes according to the aim of the experiment. Images were taken with a frequency of 3 Hz with a spatial resolution of 512x512 pixels.

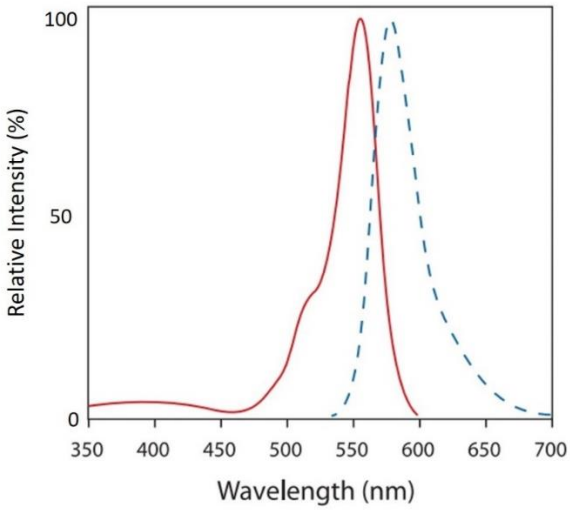

Figure 10: Excitation and emission peaks of Rhod-3 AM. The excitation peak of Rhod-3 AM is around 560 nm (red), while its emission is around 600 nm (dashed blue) [Image from Rhod-3 AM data sheet]

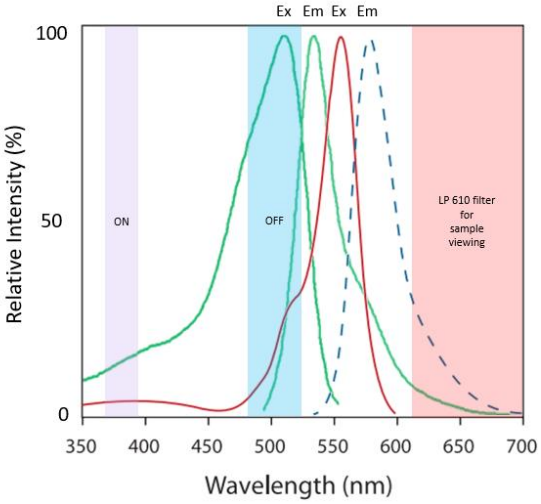

Figure 11: Scheme of the wavelengths involved in our experiments. In green, the excitation and emission spectra of GFP; in violet, the interval of activation of LiGluK2 (370-390 nm); in light blue, the interval of *optimal* inactivation of LiGluK2 (480-530 nm).

SETUP

The experimental setup consisted in an inverted microscope (Olympus IX71) geared for epifluorescence.

Sample visualization was done by means of a halogen lamp set in the transmitted light lamp housing and filtered by a 610 nm long-pass filter (Midopt, LP610-D43x2), placed in the filter pocket. The lamp was connected to an Olympus Power Supply Unit TH4-100. The rear port, on the other hand, was geared with different light sources according to the two different experimental settings we used: a filtered halogen lamp for calcium imaging and GFP excitation in the first setting, two different LEDs in the second setting. The halogen lamp was connected to an Olympus TH3 Light Power Control, while the LEDs were connected to a driver. Both were controlled manually.

The fluorescence emitted light was collected by a Digital CMOS Camera (Hamamatsu ORCA-Flash4.0 LT), positioned at the extremity of a magnification tube (4x) connected to the side port of the microscope. The camera was connected to a computer where HCImage Live software was used for recordings. LiGluK2 activation was achieved with a single mode optical fibre connected to a 375 nm laser in the first setting and with a multimode fibre connected to a 375 nm LED in the second. Since UV light is generally poorly transmitted by most objectives and other optical components, such as light guides, conveying the UV light through a fibre, rather than through the microscope's optical pathway, guarantees minimum loss of light from the source to the sample, allowing also a finer control on its intensity. By optimizing the number of wavelengths used, we have managed continuous Ca^{2+} imaging recordings and simultaneous localized channel activation: green 560 nm light (be it from a halogen lamp or LED) was used both for calcium imaging and LiGluK2 deactivation, limiting the period of activation of the channel to the period of UV illumination. Wavelengths >530 nm also favor the *trans* configuration of the azobenzene, even though the absorption of the MAG compounds becomes weaker and photoswitching requires increasingly more light. For this reason, since the excitation wavelength of Rhod-3 AM is around 560 nm, activation of LiGluk2 will occur only during 375 nm illumination.

Calcium imaging with a halogen lamp

In our very first experimental setting, activation of the channel was achieved by means of stimulation with a single mode optical fibre connected to an Oxxius LaserBoxx 375 nm laser (Figure 12). Irradiance at the sample was 5.3 mW/mm^2.

Calcium imaging was performed with a halogen lamp (Olympus U-ULS100H 100W) attached to the rear port of the microscope. The light from the halogen lamp was conveyed to the sample by means of two different filter cubes placed in the turret: one geared with an excitation filter (FF01-560/14), a dichroic filter (FF593-Di03-25x36) and a 593 nm long-pass emission filter (FF01-593/LP) for calcium imaging; the other with a 420-430 bandpass excitation filter (BP 420-480), a dichroic filter (500nm) and a 530-550 bandpass emission filter (BP530-550) for GFP visualization. All filters were from Semrock. The power registered at the sample was 2 mW for 560 nm (with an irradiance of 0,1 mW/mm^2), and 1 mW for 490 nm.

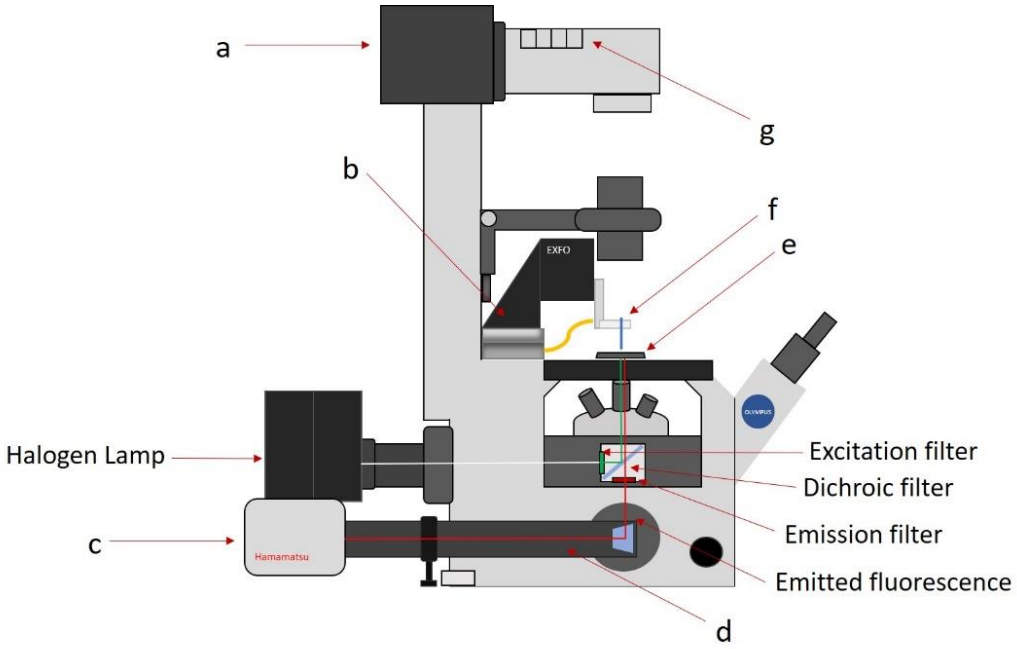

Figure 12: Calcium imaging with halogen lamp, side view. a) Halogen lamp housing; b) Headstage connected to micromanipulator for fibre positioning; c) Hamamatsu ORCA-Flash 4.0 camera; d) magnification tube (4x); e) low profile open bath chamber; f) single mode optical fibre; g) filter pocket containing 610 nm long-pass filter for brightfield sample visualization.

Calcium Imaging with a 560 nm LED

The main limitations of the first setting were the relatively low excitation of the calcium dye and the extremely low excitation of GFP with the halogen lamp illumination. In a second setting, we tried switching from a halogen light source to two LEDs (Figure 13) : a 565 nm LED (Thorlabs, M565L3, 1000 mA, 880 mW) for calcium dye excitation and a 490 nm LED (Thorlabs, M490L4, 350 mA, 255 mW) for GFP excitation. The registered power at the sample was 6 mW for the 565 nm LED (0.5 mW/mm^2 irradiance) and 5 mW for the 490 nm LED. We also switched from a 375 nm laser to a 375 nm fibre-coupled LED (Thorlabs, M375F2, 500 mA) to minimize phototoxicity and extend stimulation periods. Irradiance at the sample was 3.2 mW/mm^2. All LEDs were connected to a driver and controlled manually. Coupled to the UV LED we used a multimode (MM) optical fibre.

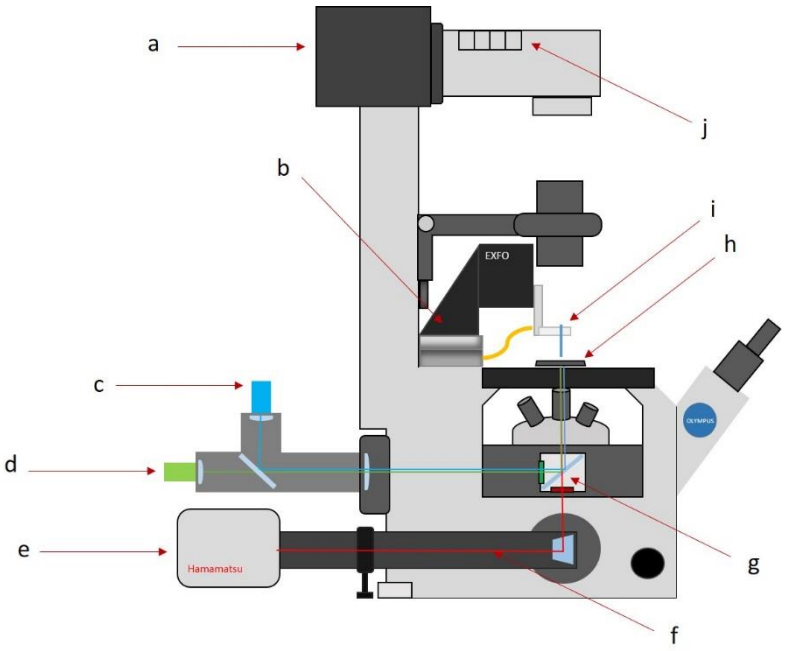

Figure 13*:* **Side view**. a) Halogen lamp housing; b) Headstage connected to micromanipulator for fibre positioning; c) 490 nm LED; d) 565nm LED; e) Hamamatsu ORCA-Flash 4.0 camera; f) magnification tube (4x); g) fluorescence cube; h) low profile open bath chamber; i) mutimode optical fibre; j) filter pocket containing 610 nm long-pass filter for brightfield sample visualization.

EXPERIMENTAL PROCEDURE

In both setups, sample and fibre positioning occurred in the same way (Figure 14). the sample was placed in a low profile open bath chamber where Ringer solution was added for recording. Due to the brevity of the recordings, no perfusion system was needed. Once the sample was positioned over the 20x objective, transfected neurons were localized thanks to the GFP reporter protein with 490 nm illumination. At this point, in brightfield, the tip of the fibre was positioned close to the transfected neuron with the help of a micromanipulator. Once positioned, illumination was switched to epifluorescence for calcium imaging. The duration of the recordings was either of 5 or 10 minutes, with different stimulation protocols. In Figure 15 we can see an example of the activity of a transfected neuron during a calcium imaging recording. LiGluK2 will be activated only during the period of 375 nm illumination, while the constant 560 nm illumination will cause it to go back to its deactivated state once UV stimulation is terminated.

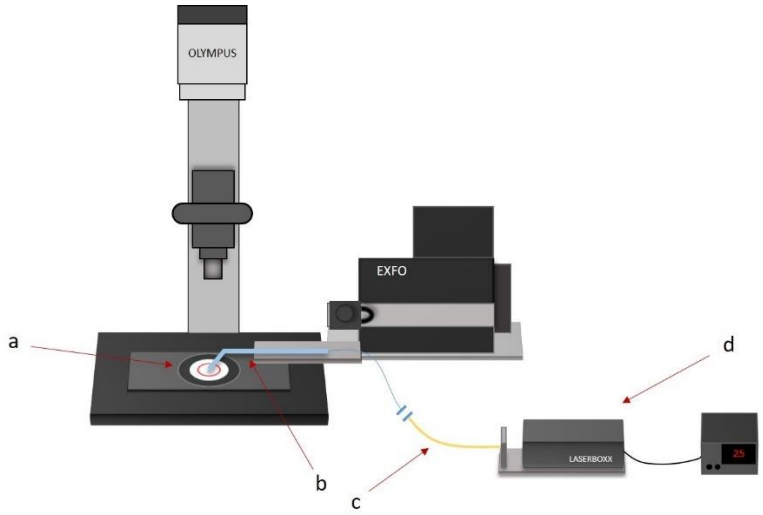

Figure 14: Sample and fibre positioning. a) sample placed inside low profile open bath chamber; b) optical fibre fixed inside glass capillary is positioned over the neuron of interest by means of the micromanipulator; c) single-mode or multimode optical fibre spliced to patch cable; d) 375 nm laser (Oxxius Laserboxx) or a 375 nm fiber-coupled LED.

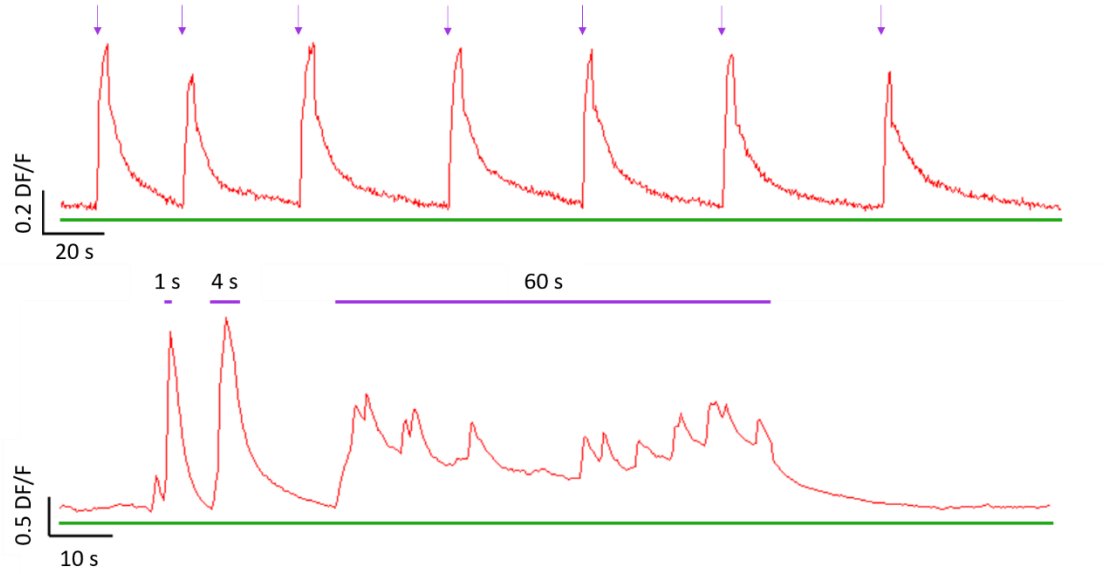

Figure 15: Example of calcium transients in transfected neurons during UV illumination. In the top trace we can see how pulses of 1 s led to single calcium transients. In the bottom trace, on the other hand, we can see what can happen with longer periods of stimulation, where the neuron responds with multiple transients. In both cases, the green line under the trace represents the constant 560 nm illumination used in calcium imaging recordings, while the violet arrows and lines represent the 375 nm stimuli. Fluorescence variation is expressed as ΔF/F.

OPTICAL FIBRES

Two different kinds of optical fibres were used in our experiments:

a) Single Mode (SM) fibres
b) Multimode (MM) fibres

The SM fibres we used (SM300, 0.13 NA, Thorlabs) had an operating wavelength from 320 to 430 nm and consist of an undoped, pure silica core surrounded by a depressed, fluorine-doped Ø125 µm cladding and a dual acrylate coating (245±15 µm).

MM fibres (FT400UMT, 0.39 NA, Thorlabs), on the other hand, had an operating wavelength of 300-1200 nm. They are characterized by a silica core with a diameter of 400 ± 8 µm and present a TECS hard cladding (425 ± 10 µm) and Tefzel coating (730 ± 30 µm). Coating was stripped before splicing.

All fibres were spliced to a suitable fibre patch cable by means of a single fibre fusion splicer (FSU 995 FA, Ericsson). The patch cables used were a Single Mode Fibre Patch Cable 320-430 nm (P1-305A-FC-2, Thorlabs) and a custom Multimode Fibre Patch Cable (FT400UMT, Thorlabs).

Passing from a SM to a MM fibre was necessary when using a UV LED, since a larger core is needed to carry a weaker light to the sample. In this passage to a larger core, tapering of the fibre was deemed necessary in order to reach a more localized stimulation. The final size of the MM fibre tip was around 9µm.

Tapering of the fibre indeed led to a great difference in the dimension of the area of illumination, passing from a spot with a diameter of roughly 300 µm to one of about 40 µm (Figure 16-Figure ***17***), allowing us to eventually confine the spot of light to the soma of a single transfected neuron in cultures that were not too densely populated. In experiments with the SM fibre, on the other hand, stimulation was done on a small area comprising more neurons, and, therefore, cannot be defined as localized stimulation.

All optical fibres were then fixed inside a bent glass capillary for support.

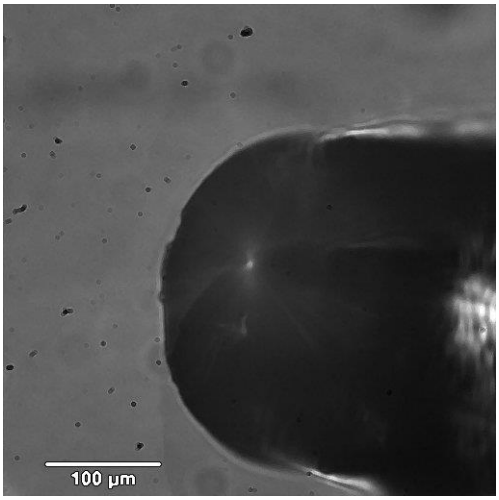

Figure 16: Tip of the untapered single mode fibre, 80x magnification

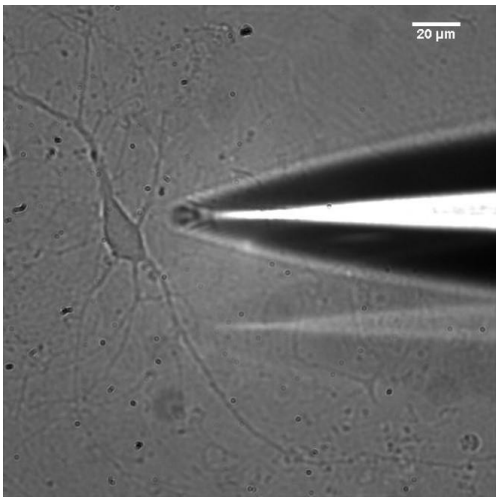

Figure 17: Multimode tapered fibre next to a neuron. 80x magnification

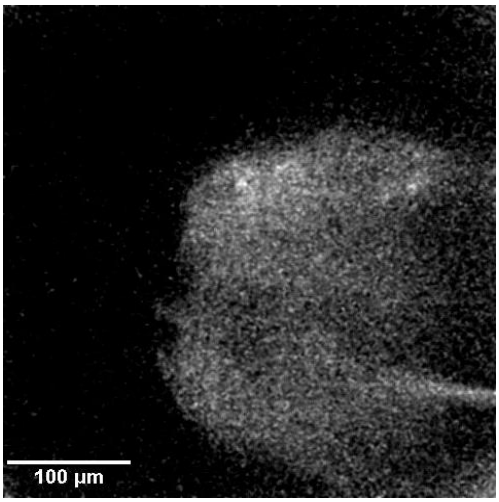

Figure 18: Dimension of the spot of light exiting the single mode fibre, 80x magnification.

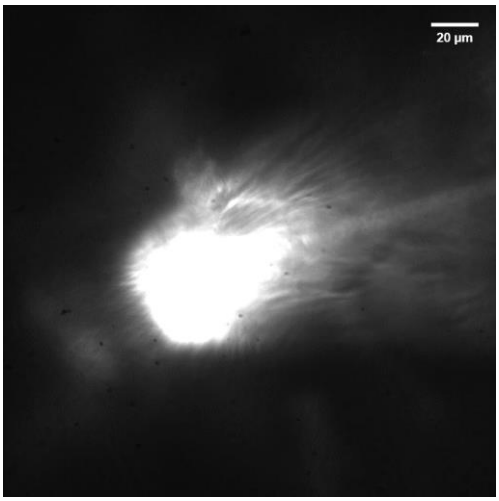

Figure 19: Dimension of the spot of light exiting the tapered multimode fibre, 80x magnification.

RESULTS

We managed to probe small networks of neurons by combining stimulation of LiGluk2 and calcium imaging.

Dissociated neuronal networks from rat hippocampus were cultured for 1 week before proceeding to transfection (Figure 20A). As described in the Methods section, successfully transfected neurons could be detected by GFP expression (Figure 20B). Cells were loaded with the calcium dye Rhod-3 AM (Figure 20C). Activation of LiGluK2 leads to different kinds of neural activity according to the physiology and the connections of the neurons involved.

FIRST SETTING

In our first experiments, we used a filtered halogen lamp for calcium imaging and a single mode optical fibre connected to a 375 nm laser for LiGluK2 activation. the paradigm for stimulation consisted in a single period of stimulation of 30s, in order to analyse more accurately the before and after effects of activation of LiGluK2 receptors. As already mentioned, the untapered fibre illuminated an area of around 300 µm in diameter, and therefore cannot be defined as localized stimulation. However, this allowed us to

stimulate more transfected neurons contemporarily. In Figure 20, for example, we can see the effect of a 30s second stimulation on 3 transfected neurons.

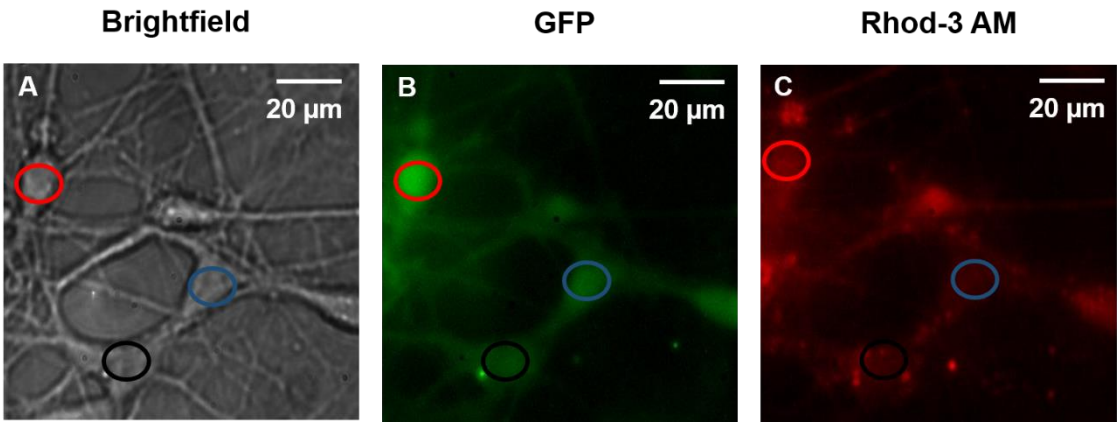

Figure 20: Inducing activity in a network of three transfected neurons. A. Brightfield image of three neurons; **B.** LiGluK2 transfection reporter GFP; **C.** Rhod-3 AM signal

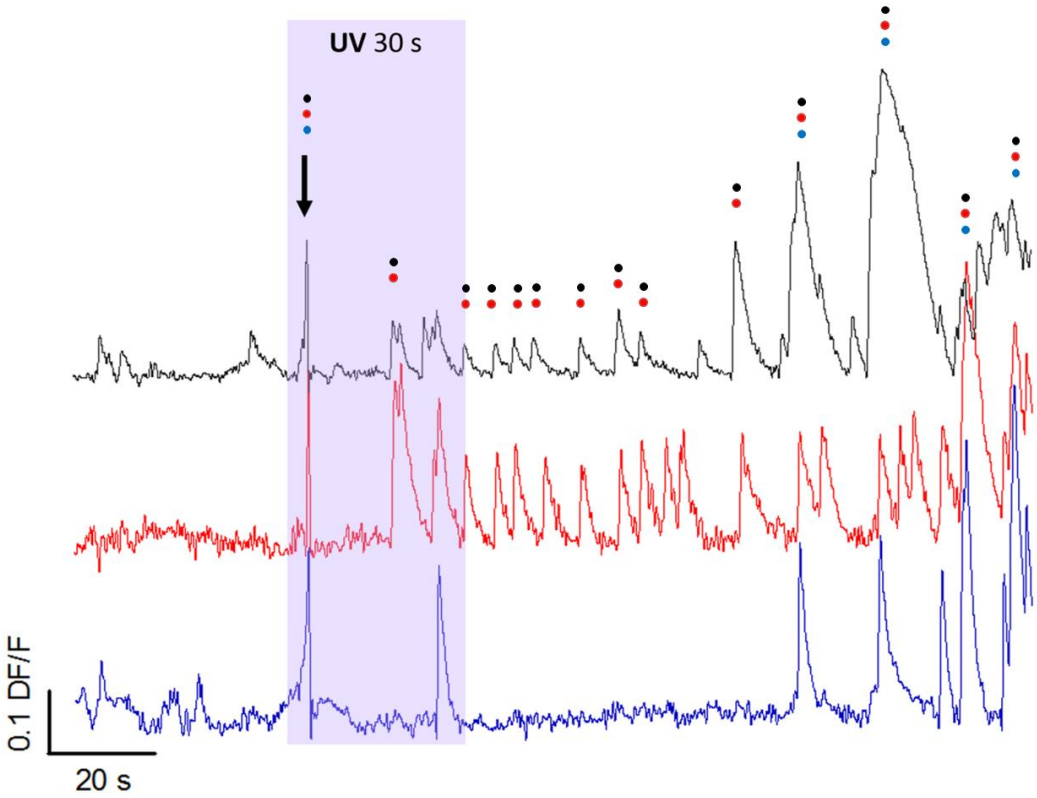

Figure 21: Inducing activity in a network of three transfected neurons. Induced calcium transients recorded in the neurons in Figure 20 in three different neurons (circled in red, black and blue). Activation

of the 375 nm laser leads to a synchronous event (indicated by the black arrow) followed by an increase in the number and frequency of the peaks. Synchronous events are indicated by the dots.

Before UV illumination, no spontaneous activity was present in the three neurons. In Figure 21, we can see the optical traces of the three transfected neurons (circled in Figure 20 A-C in black, red, and blue). Activation of the 375 nm laser leads to a synchronous event (indicated by the black arrow) followed by an increase in the number and frequency of the peaks. The occurrence of calcium transients in different neurons was poorly synchronous before activation of LiGluK2 receptors and significantly increased following their activation.

A second kind of activity we observed was global bursting in groups of anatomically and functionally tightly connected neurons (Figure 22C). Indeed, in some experiments we did not observe the single layer of cells usually present in dissociated neuronal cultures, but a dense assembly of neurons, possibly forming a multi-layered structure (Figure 22A, Figure 24A). In these experiments the fluorescence emitted by the GFP was bright and extending all over the neuronal assembly (Figure 22B, Figure 24B), suggesting that most neurons were successfully transfected with LiGluK2 receptors. UV illumination led to a delayed global burst likely to involve a large fraction of the neurons (Figure 23). At the top of the large and global optical transients, we observed smaller synchronous events with the usual time course of calcium transients from single neurons.

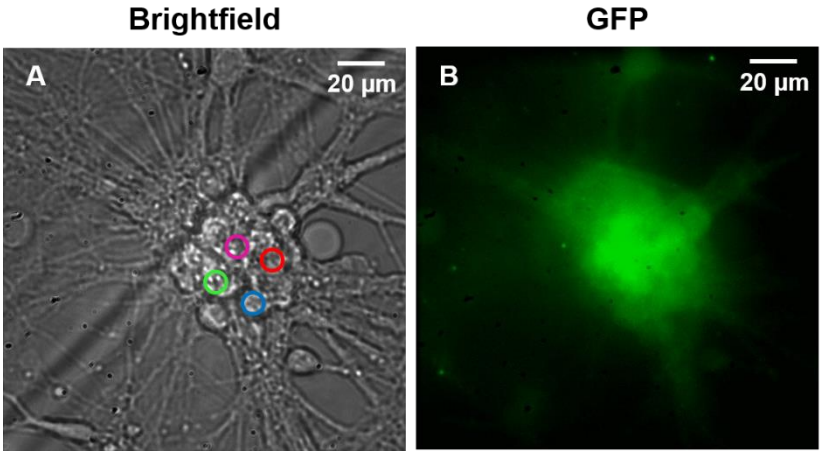

Figure 22: Delayed burst in group of neurons after stimulation. A. Brightfield image of a small cluster of neurons; the soma of four transfected neurons is circled in different colours; **B.** Transfection: GFP reporter shows that the LiGluK2 DNA has been successfully expressed;

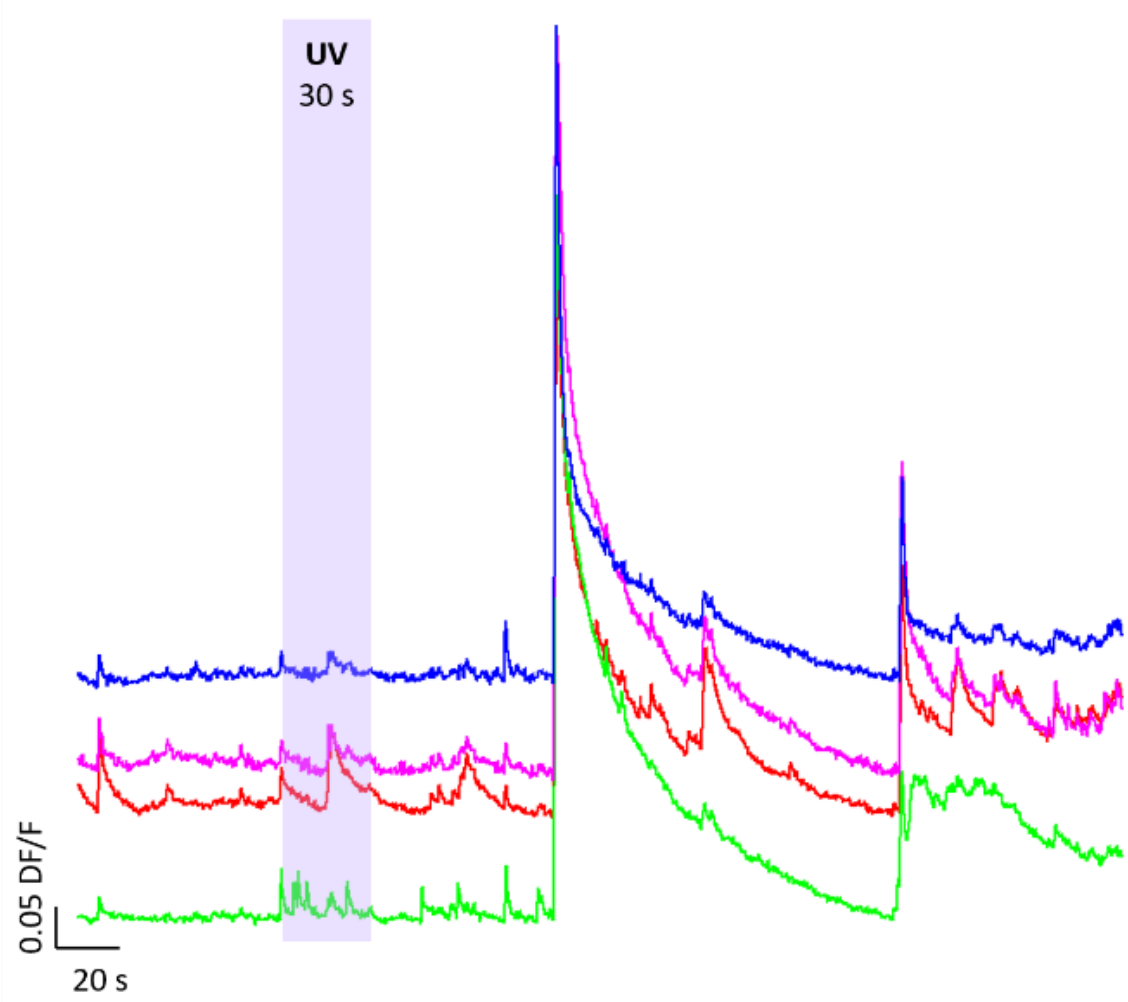

Figure 23: Delayed burst in group of neurons after stimulation. A 30 s stimulation with the UV light initiates the activation of the receptors. The signaling cascade leads to a synchronous burst. Fluorescence variation expressed as ΔF/F.

In some cases (Figure 25), the activation of LiGluK2 led to a significant steady increase of intracellular calcium. Rhod-3 AM emitted fluorescence was much greater 3 minutes after the activation of the receptor (Figure 24C). This increase of intracellular calcium led to cell death within 3-5 minutes. In a parallel series of experiments (carried out by Xiaoyun Li and Renza Spelat), using ratiometric calcium imaging with the calcium indicators Fluo-4 and Fura-Red, and in the absence of transfection with LiGluK2 receptors, we quantified the level of intracellular calcium leading to cell death, which ranged from 400 to 600 nM. Therefore, we estimate that the value of intracellular calcium causing cell death in the experiment of Figure 24-25 is about and above 500 nM.

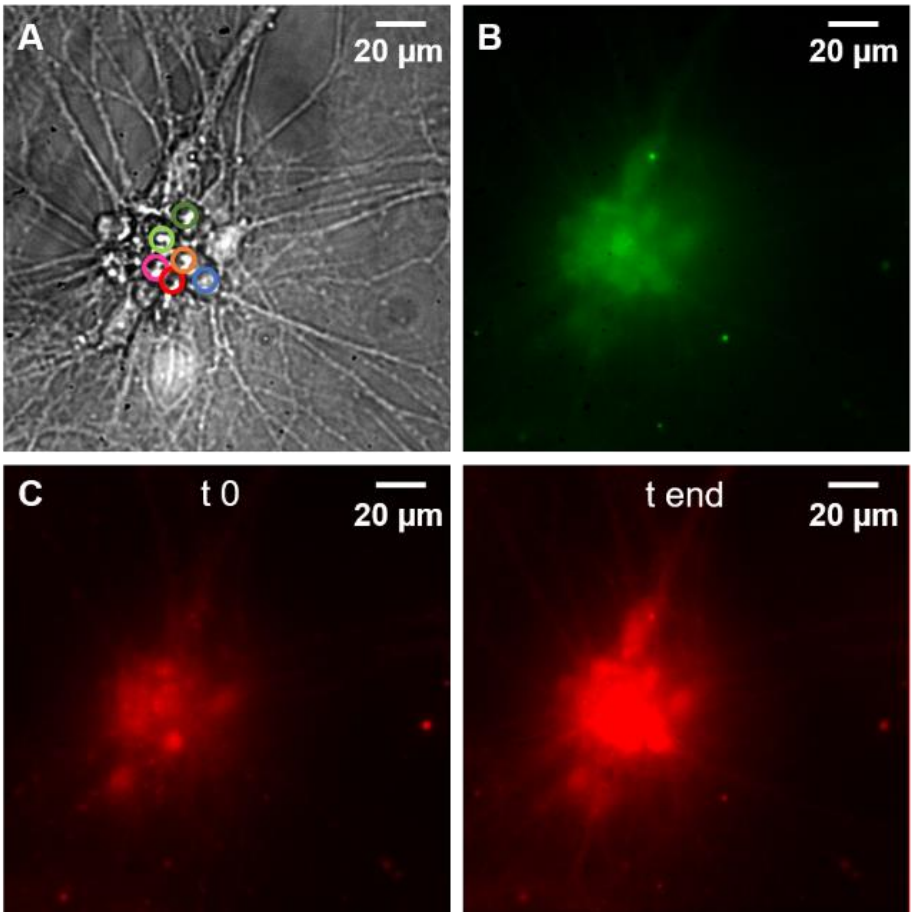

Figure 24: **Stimulation leads to sustained calcium influx**. **A**. Brightfield; **B.** Transfection, GFP expression; **C.** Rhod-3 AM fluorescence at beginning (t_0) and end of recording (t_{end}) (10 minutes).

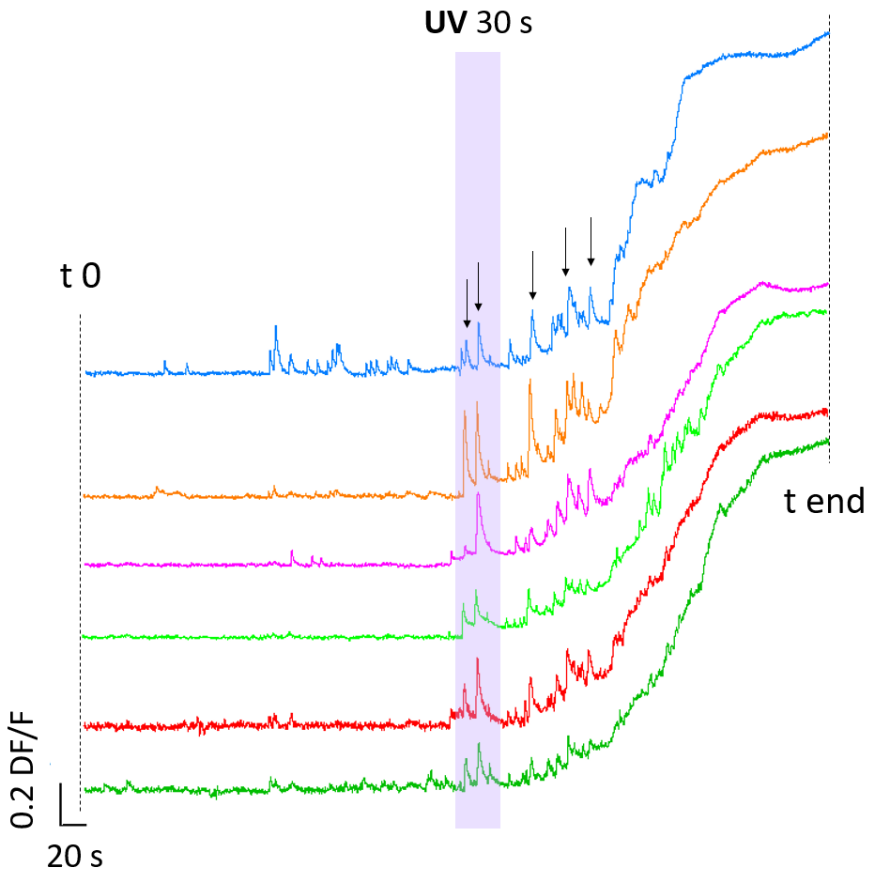

Figure 25: Stimulation leads to sustained calcium influx. Fluorescence variation expressed as ΔF/F: after UV stimulation cells initially show synchronous calcium transients (arrows), but continuous activation leads to a steady calcium influx and, finally, cell death.

These experiments allowed us to have a good time window to compare the activity before and after UV stimulation. Across all experiments (n=20), what we found was a significant increase in the number of calcium peaks after stimulation. Collected data from 40 neurons shows that the mean number of calcium transients (larger than 0.1) in a time window of 5 minutes before and after activation of LiGluK2 increased from 5.3±1.2 to 16.5±2.6 (Figure 26), passing from a mean 1.07 peaks/min to 3.3 peaks/min.

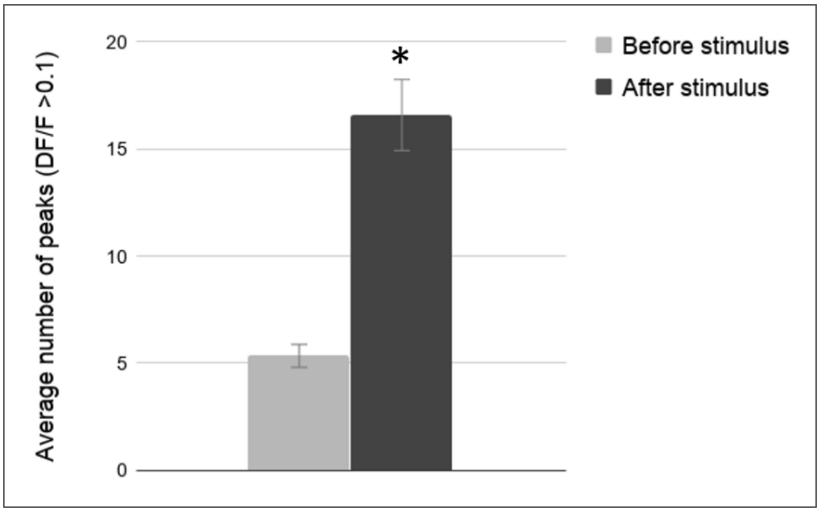

Figure 26: Statistics of effects of LiGluK2 across experiments. Histogram of the average number of peaks in neurons (n=40) across 20 experiments, before (light grey) and after (dark grey) stimulation with 375 nm laser (Mann-Whitney U Test, $^{*}P < 0.001$).

SECOND SETTING

In our second setting, LEDs were implemented both for calcium imaging and for neuron stimulation. Due to the lower maximum intensity of the UV LED (4.2 mW), a multimode optical fibre was required. Because of the larger core of this kind of fibre, tapering was deemed necessary.

The advantage of a tapered fibre is a more confined and localized stimulation, allowing us to activate single transfected neurons among small neural networks. While in our first setting stimulation only occurred mid-recording, in these experiments we followed different stimulation protocols:

1. One second single pulses
2. Pulses of increasing duration
3. A single pulse at the beginning of recording

1. One second single pulses

During these recordings, single pulses of 1 s were delivered. The transfected neurons were isolated or among small neuronal groups.

For each pulse delivered, the neuron responded with a calcium transient, that could lead to activation of the surrounding cells even in the absence of prior spontaneous activity.

An example is shown in Figure 15. Constant illumination with 560 nm LED is depicted by the green line beneath the trace, while the single UV pulses are represented by the violet arrows. Across experiments (n=43), 86,1 % of transfected neurons responded. The mean ΔF/F across experiments (in a total of 170 measurements stimulus-response) was 1.5±0.05. The mean variation of fluorescence after stimulation was 1.9 ±0.2 ΔF/F at the beginning of the recording and 1.4±0.2 at the end, with a 26% mean decrease.

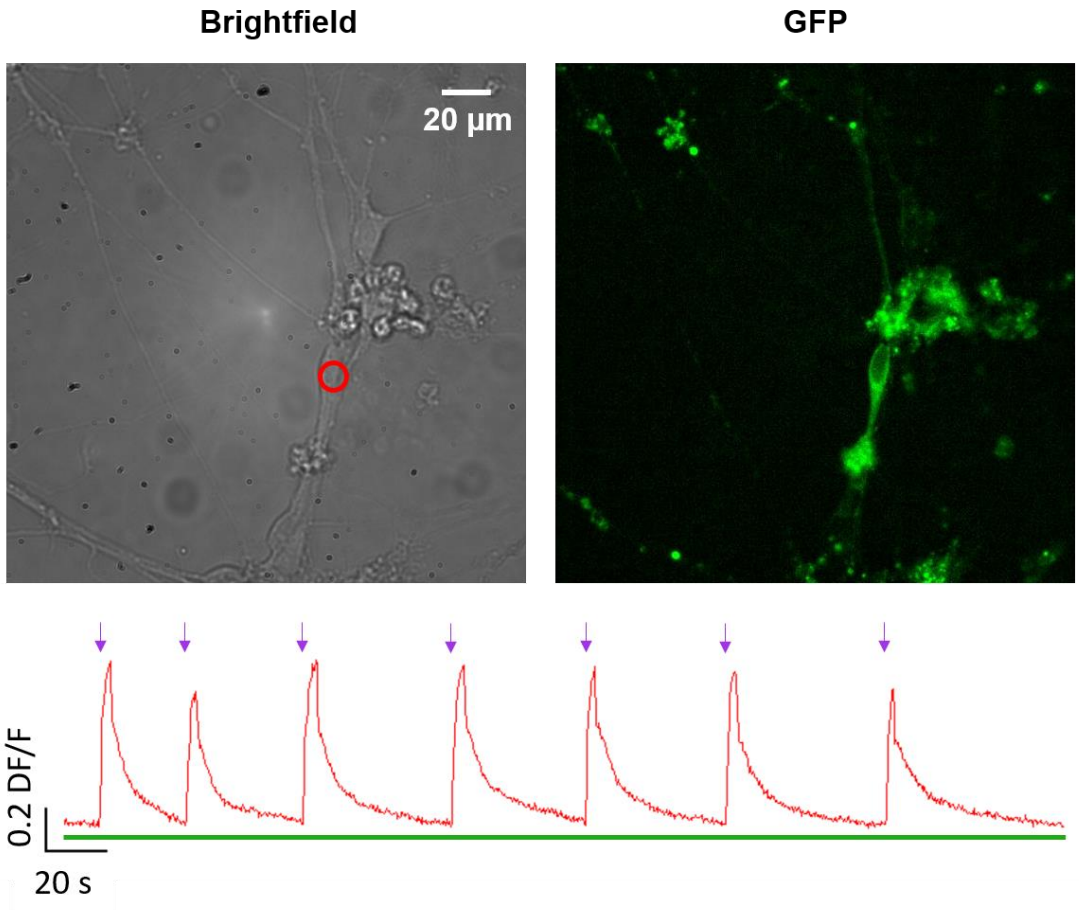

Figure 27: Single pulse stimulation elicits single calcium transients. Transfected neuron is circled in red. Each arrow in the optical trace represents a UV pulse of one second. The green line under the trace represents the constant 560 nm illumination used in calcium imaging recordings. Fluorescence variation is expressed as ΔF/F.

2. Pulses of increasing duration

The use of a stimulation protocol with pulses of increasing duration has allowed us to see what occurs to the transfected neuron during longer periods of stimulation. In these

experiments we observed two kinds of behavior during 375 nm illumination: single prolonged calcium transients (Figure 28) and multiple transients (Figure 29). Single prolonged calcium transients were the most frequent across experiments, while multiple calcium transients during prolonged UV illumination were found less frequently, in around 20% of experiments (n=20).

It was not completely unexpected that towards the end of the recordings, when the pulses were the longest, the neuronal responses were smaller in amplitude compared to the first responses solicited. Across 20 experiments (a total of 20 stimulated neurons), the mean ΔF/F at the beginning of the recording was 2.5±0.1 decreasing to 1.2±0.4 ΔF/F at the end, with a 56% mean decrease. There was great variability in the trend of ΔF/F during these recordings, but we can affirm that there was a decrease in the majority of cases (87.5%) and that this decrease wasn't always linear.

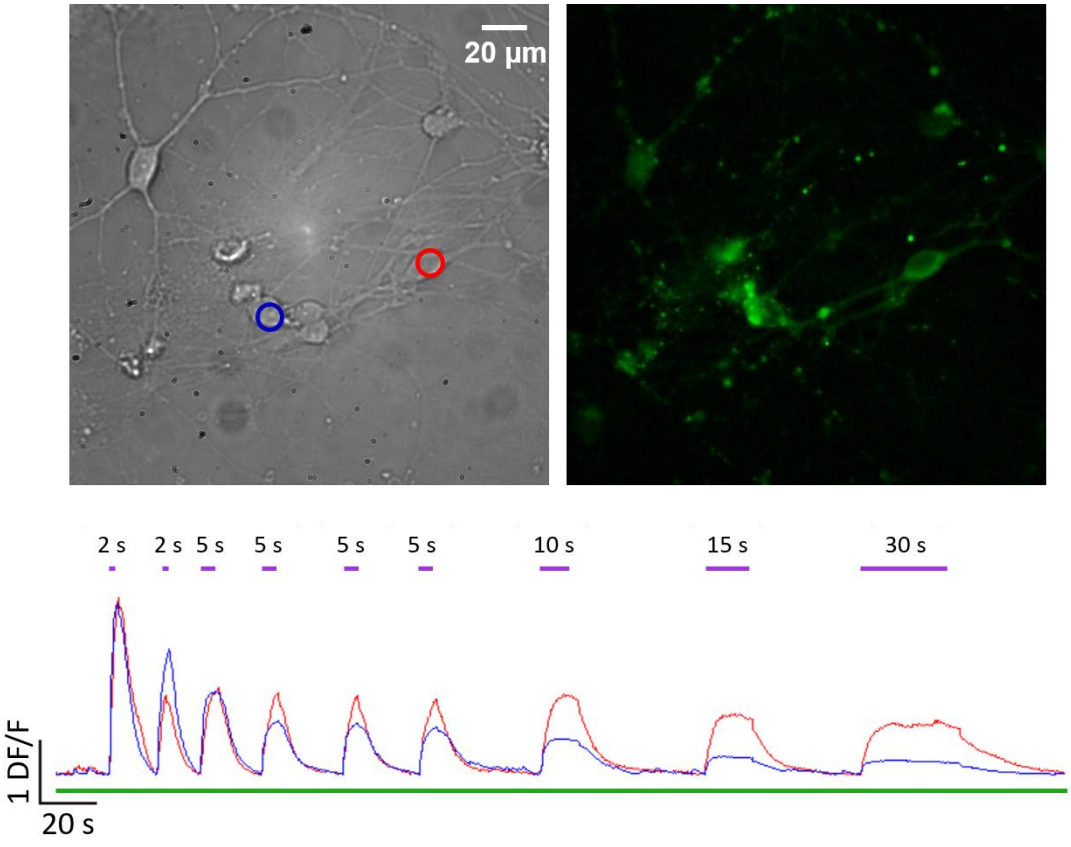

Figure 28: UV illumination leads to prolonged calcium transients. In this experiment, we can see two transfected neurons (circled in blue and red). UV stimulation was increased from 2 to 30 s. Constant 560 nm illumination is represented by the green line under the optical traces.

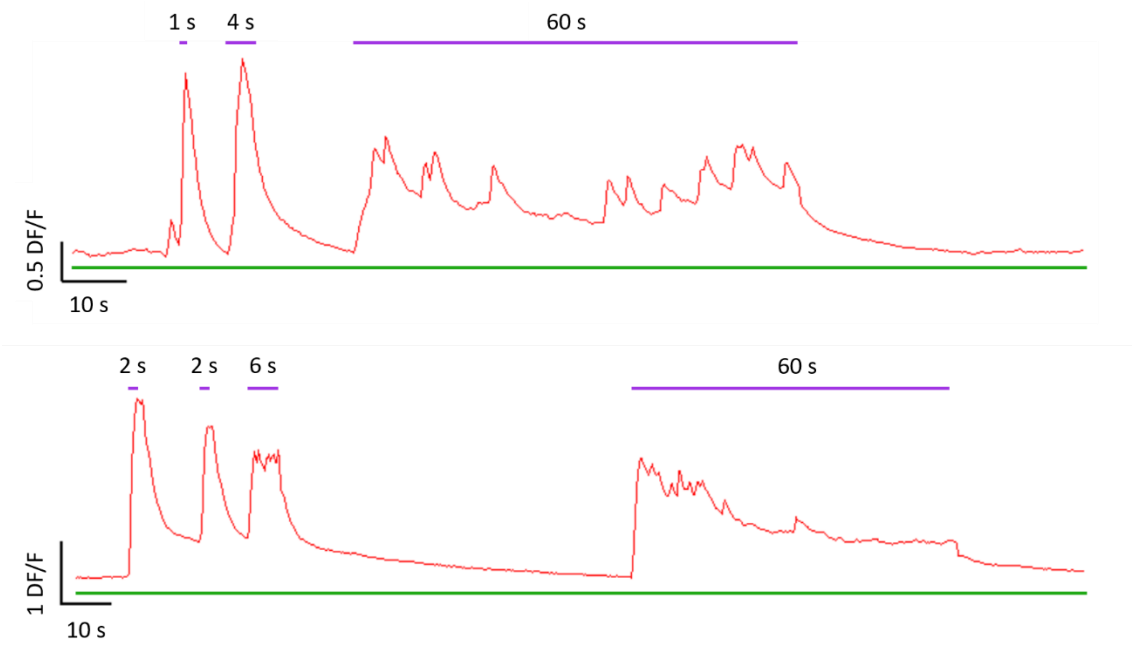

Figure 29: Multiple calcium transients during UV stimulation. In some cases, multiple peaks were visible during UV stimulation over long periods (60 s). Constant 560 nm illumination is represented by the green line under the optical traces.

3. Single pulse stimulation at the beginning of recording

Once the effect of the UV stimulation was assessed, we decided to perform a single stimulation at the beginning of the calcium imaging recordings. In cases like the ones depicted in Figure 30 and Figure 32, we worked on small networks where only one neuron was clearly and well transfected (Figure 30B): UV illumination activated the single transfected neuron and therefore it was possible to analyze its effect on the network activity. Following activation of LiGluK2 receptors, two large calcium transients were detected in the transfected neuron (indicated by the black arrow in Figure 31) which in turn evoked similar calcium events in a nearby neuron (blue arrow). Once initiated, this network activity could be clearly seen for some minutes involving several neurons in the network. In the first five traces, we can see how the activation of the transfected neuron leads to a cascade of activation in the surrounding network. In the last two traces, on the other hand, we can see how two neurons already presenting spontaneous activity experience a variation in frequency and amplitude of the calcium events, consistent with the results obtained in our other experiments.

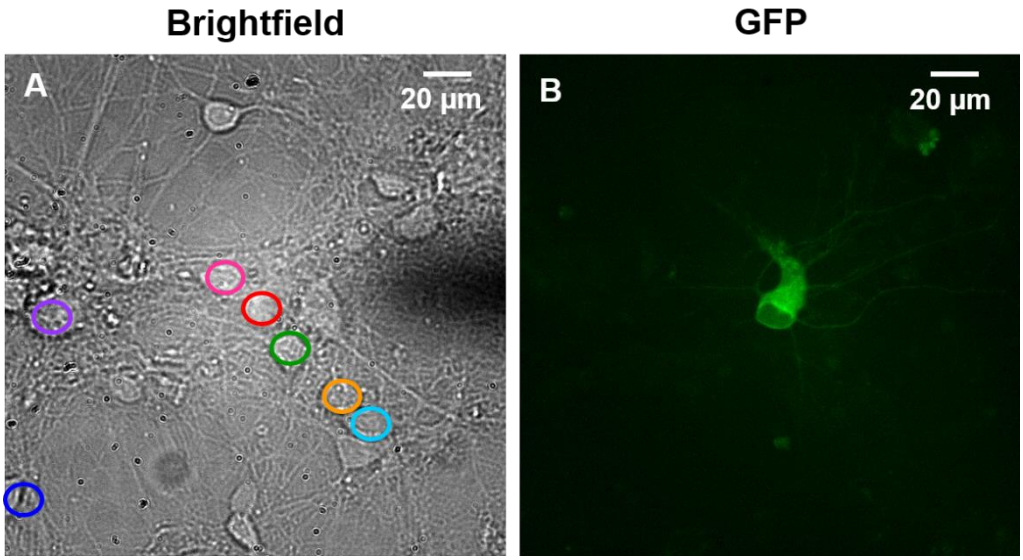

Figure 30: Single neuron stimulation. A. Brightfield**,** transfected neuron is circled in red; **B.** Transfected neuron.

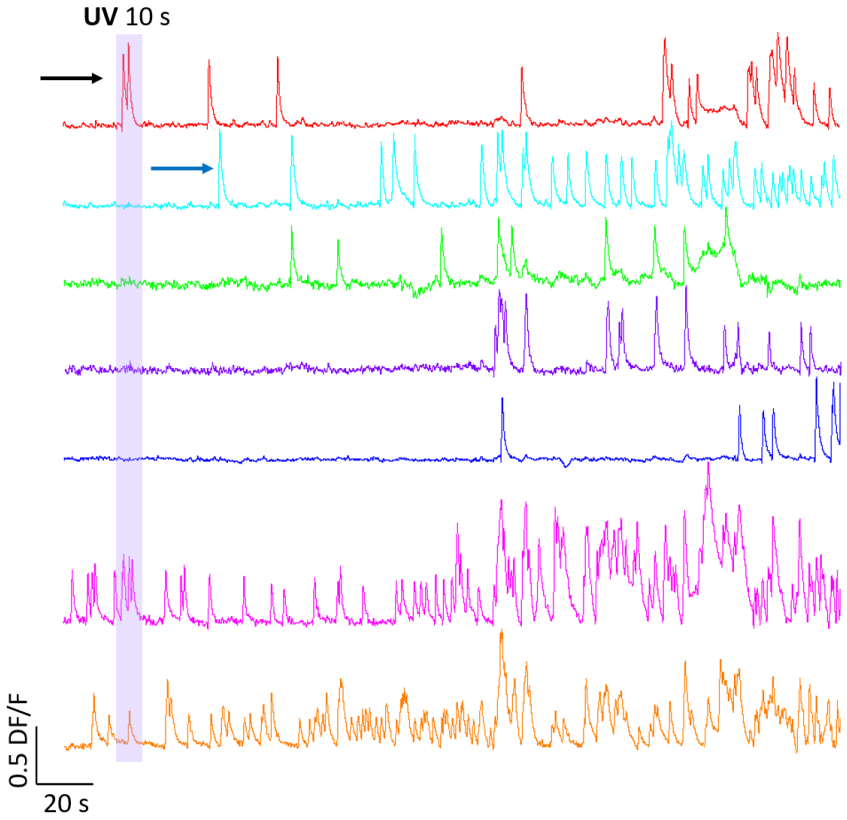

Figure 31: Single neuron stimulation. 10 s UV stimulation led to activation of the transfected neuron, which in turn causes an activation cascade of the surrounding neurons. In neurons where activity was

already present, stimulation and network connectivity led to an increase in the frequency and amplitude of the calcium events. Fluorescence variation expressed as ΔF/F.

In a similar experiment (Figure 32-Figure **33**), a single transfected neuron was stimulated for 10s. In this case also, a calcium transient is evoked in the targeted neuron and propagates to the surrounding cells in the network, causing synchronized activation in cells that showed no previous spontaneous activity.

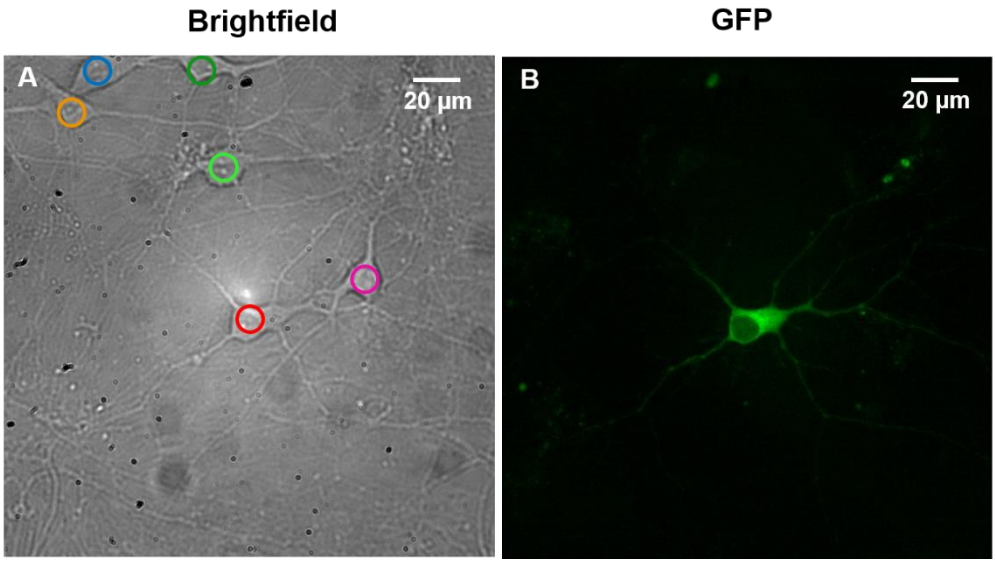

Figure 32: Single neuron stimulation. A. A small group of neurons in brightfield, transfected neuron is circled in red. **B.** Transfected neuron.

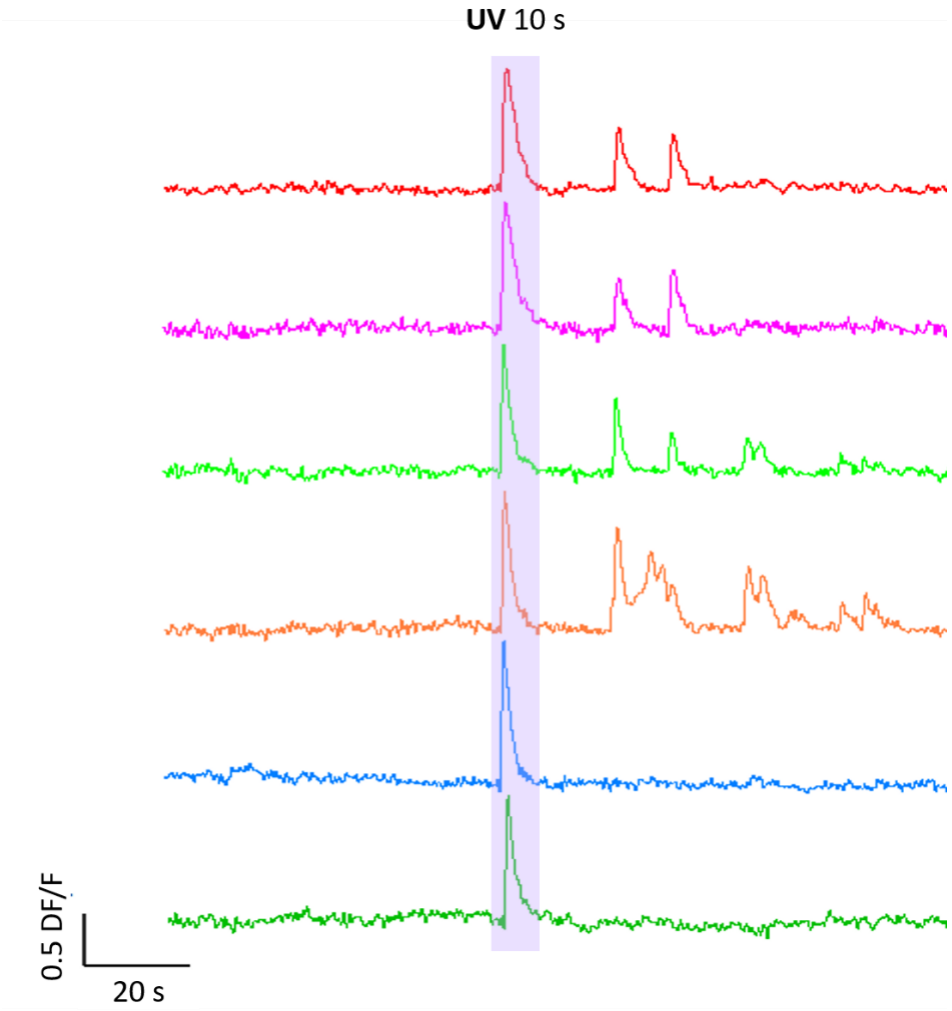

Figure 33: Single neuron stimulation. UV stimulation (10 s) leads to the initiation of activity in a small network of neurons. Activation of the transfected neuron starts synchronized calcium transients. The colour of each trace refers to neurons circled in Figure 32.

CONTROL EXPERIMENTS

Calcium imaging was performed on wild-type hippocampal neurons and the various stimulation paradigms were applied. What we confirmed was that UV illumination on its own is not responsible for the induced neuronal activity. Across experiments, no neuron (n=20) showed induced activation nor variation in its spontaneous activity.

DISCUSSION

We devised a method to couple *in vitro* optogenetics with calcium imaging in order to combine optical stimulation with optical sensing. Delivery of the UV light through an optical fibre, rather than through the microscope's optical pathway, guaranteed minimum loss of light from the source to the sample, since UV light is generally poorly transmitted by most objectives and other optical components. Furthermore, we have managed continuous Ca^{2+} imaging recordings and simultaneous localized channel activation by optimizing the number of wavelengths used: green 560 nm light (be it from a halogen lamp or LED) was used both for calcium imaging and LiGluK2 deactivation, limiting the period of activation of the channel to the period of UV illumination.
Here we discuss the results obtained with the two setups and the possible applications of the technique.

Calcium Imaging with a Halogen Lamp

Halogen lamps are a cheaper and more stable alternative to xenon an mercury lamps and present a reduced phototoxicity [112]. However, we found that the excitation of the fluorophores Rhod-3 AM and GFP in our experiments would require longer exposure times to obtain an optimal signal.
These experiments consisted in 10-minute recordings, where UV stimulation was performed for 30 s mid-recording. This allowed us to have two good temporal windows of five minutes to evaluate activity before and after LiGluK2 activation. Activation of LiGluK2 was done with a single mode optical fibre connected to a 375 nm laser. The fibre was not tapered, so stimulation was not confined to a single neuron and could cover an area comprising more cells, allowing the stimulation of more transfected neurons contemporarily. Calcium transients were induced even in neurons that showed no prior spontaneous activity.
We identified three main regimes present in the analysed small neuronal networks after LiGluK2 activation: firstly, sustained neuronal firing with different levels of synchrony across neurons; secondly, early excitation with delayed synchronous bursting; thirdly, global firing triggering a massive increase of intracellular calcium leading to cell death. Two main mechanisms are at the origin of the observed dynamic regimes: firstly, the random connectivity of the analysed neuronal network together with cell culture intrinsic

variability, and secondly the stochasticity in the number and degree of transfection with the LiGluK2 channels.

As for the massive intracellular calcium increase, this is probably due to the influx of calcium through voltage-dependent calcium channels and release from the internal calcium stores rather than the activation of LiGluK2 only. This is confirmed by the fact that all cells, not only those transfected, are affected. This sign of suffering could be caused by phototoxicity but is more likely ascribed to the state of health of the cultured cells, since in experiments with a stronger light source (i.e. LEDs) there were no gross signs of phototoxic effects. In other experiments with this setup, however, blebbing was found to occur. Considering that we did not see this phenomenon neither in control recordings of the same length (10 minutes), nor in experiments with the second setup, we arrived at the conclusion that this sign of phototoxicity was due to the use of the UV laser.

Calcium Imaging with a 560 nm LED

The relatively low excitation of the calcium dye and the extremely low excitation of GFP with the halogen lamp illumination, made us consider another light source, LEDs. This resulted in much greater fluorescence both of Rhod-3 AM and GFP at low times of exposure ($\leq$ 300 ms). Because of the phototoxicity caused by the UV laser, we decided to switch to a 375 nm fibre-coupled LED. In this case, the fibre used was a multimode optical fibre, tapered with the objective of reaching a localized stimulation of single transfected neurons.

These experiments consisted in shorter 5-minute recordings, where 3 different stimulation protocols were applied. Approach to analysing the results was different according to the stimulation paradigm.

With one second pulses we were interested in seeing how a localized response could be evoked and how this response would vary after each stimulus along the recording, so we considered the amplitude, in terms of $\Delta F/F$ variation, of each response. We found that the elicited calcium transients presented similar $\Delta F/F$, and that there was no significant variation between the beginning and the end of the recording. We also found that across experiments (n=43) 86,1% of transfected neurons responded.

With pulses of increasing duration, similarly, we wanted to verify what occurred during longer periods of illumination and how the cells would respond. In this case we found two different kinds of response: single prolonged calcium transients and multiple

transients, though the first were the most common result of stimulation. In this case ΔF/F tended to decrease in time, with a 56% mean decrease.
The final stimulation protocol was similar to the one used in the first setup, where a single period of stimulation was performed at the beginning of the recording. In this case the period was of 10 seconds. UV stimulation activated the transfected neuron which in turn caused a cascade of activation in the surrounding network. The synchronicity of events generally increased, and activity was elicited also in neurons that did not present spontaneous transients.

There is apparently a difference in the activity of the transfected neurons in the 2 sets of experiments, probably due to the continuous stimulation with UV pulses: in the first setting, after a single stimulation activity continued in the transfected neuron; in the second setting, on the other hand, activity was present only during LiGluK2 activation. The fact that this could be due to the stimulation paradigm is confirmed by the experiments in the second setting, when only a brief period of 375 nm illumination was given, where the transfected neuron continued to present calcium transients after activation. Nevertheless, in both sets of experiments activation of transfected neurons led to an increase in the number of calcium transients in the neurons under exam.
We also found variability of the latency with which surrounding neurons respond to the activation of the transfected neurons: in some cases, the event was synchronous, while in other experiments this delay was significantly larger even up to 20-30 seconds. This variability can be rationalized by the specific connectivity of the neuronal network under observation and the general state of health of the cultured cells. Moreover, the variability in the activity elicited by the activation of the transfected neurons can be ascribed not only to the random connectivity of the neural network, but also to the physiological properties of the neurons involved.
This method can also be used with other biologically relevant light-gated ion channels. In our case, we have analysed the effect of activation of LiGluK2 in isolated neurons and in small networks, where the receptor maintains the same properties as its native counterpart. But information on the effect of the introduction of point mutations in the network connectivity can be collected and can complement, for example, electrophysiological data from patch clamp experiments. A key feature of the PTL-based approach is that genetic changes may be made to the protein of interest while maintaining the ability to specifically manipulate it through photoswitch conjugation. For example,

one may make mutations to various functional or regulatory sites within LiGluR without disrupting its ability to become photo-activated by MAG, thus enabling direct testing of the role of the mutated residues in receptor function. This represents a major improvement in terms of temporal and spatial control over classical knock-in approaches [52].
In addition to this, it would be interesting to transfect the receptor in hippocampal slices and eventually combine this method with patch clamping. Primary cell cultures are a good place to start, but the variability of the cell cultures and the networks that they form make organotypic slices, which maintain the tissue's architecture, a candidate for future experiments

CONCLUSIONS

The combination of optical activation of neurons and optical sensing has proved to be an efficient method for controlling and studying small networks of neurons *in vitro*.
The present investigation shows that it is possible to analyse cultured neuronal networks with optogenetic tools, where light is used to open and close ionic channels that have conduction properties identical to those of native channels. LiGluK2, as a matter of fact, maintains all the key features of its native counterpart GluK2, preserving a channel conductance of 25 pS, much higher than the 1 pS of ChRs. Compared to classic optogenetics, the PTL-based approach allows to eventually probe the function of specific receptor subtypes, rather than controlling cellular excitability alone. This method could also be used on organotypic cultures, where the architecture of the tissue is maintained, but also to rapidly assay the functionality of newly designed PTLs.

BIBLIOGRAPHY

1. Contractor A, Mulle C, Swanson GT. Kainate receptors coming of age: Milestones of two decades of research. Trends Neurosci. 2011;34(3):154–63. Available from: http://dx.doi.org/10.1016/j.tins.2010.12.002

2. Lerma J, Marques JM. Kainate receptors in health and disease. Neuron. 2013;80(2):292–311. Available from: http://dx.doi.org/10.1016/j.neuron.2013.09.045

3. Volgraf M, Gorostiza P, Numano R, Kramer RH, Isacoff EY, Trauner D. Allosteric control of an ionotropic glutamate receptor with an optical switch. Nat Chem Biol. 2006;2(1):47–52.

4. Reiner A, Levitz J, Isacoff EY. Controlling ionotropic and metabotropic glutamate receptors with light: Principles and potential. Curr Opin Pharmacol. 2015;20:135–43. Available from: http://dx.doi.org/10.1016/j.coph.2014.12.008

5. Kramer RH, Mourot A, Adesnik H. Optogenetic pharmacology for control of native neuronal signaling proteins. Nat Neurosci. 2013 Jun 25;16:816. Available from: http://dx.doi.org/10.1038/nn.3424

6. Mohanty SK, Group P, Lakshminarayananan V, Science V, Arbor A. HHS Public Access. 2015;62(12):949–70.

7. Szobota S, Isacoff EY. Optical Control of Neuronal Activity. Annu Rev Biophys. 2010;39(1):329–48. Available from: http://www.annualreviews.org/doi/10.1146/annurev.biophys.093008.131400

8. Fenno L, Yizhar O, Deisseroth K. The Development and Application of Optogenetics. Annu Rev Neurosci. 2011;34(1):389–412. Available from: http://www.annualreviews.org/doi/10.1146/annurev-neuro-061010-113817

9. Reiner A, Levitz J, Isacoff E. Bringing optogenetics to the synapse. Neuron. 2013;79(2):209–10. Available from: http://dx.doi.org/10.1016/j.neuron.2013.07.009

10. Reiner A, Isacoff EY. Photoswitching of cell surface receptors using tethered ligands. Methods Mol Biol. 2014;1148:45–68. Available from: https://doi.org/10.1007/978-1-4939-0470-9_4

11. Aston-Jones G, Deisseroth K. Recent advances in optogenetics and pharmacogenetics. Brain Res. 2013;1511:1–5. Available from: http://dx.doi.org/10.1016/j.brainres.2013.01.026

12. Mohanty SK, Lakshminarayananan V. Optical techniques in optogenetics. J Mod Opt. 2015 Jul 12;62(12):949–70. Available from: https://doi.org/10.1080/09500340.2015.1010620

13. Spudich JL. The multitalented microbial sensory rhodopsins. Trends Microbiol. 2006 Nov 1;14(11):480–7. Available from: https://doi.org/10.1016/j.tim.2006.09.005

14. Sakmar TP. Structure of rhodopsin and the superfamily of seven-helical receptors : the same and not the same. Curr Opin Cell Biol. 2002;14:189–95.

15. Shichida Y, Yamashita T. Diversity of visual pigments from the viewpoint of G protein activation - Comparison with other G protein-coupled receptors. Vol. 2, Photochemical & photobiological sciences : Official journal of the European Photochemistry Association and the European Society for Photobiology. 2004. 1237-1246 p.

16. Nagel G, Szellas T, Huhn W, Kateriya S, Adeishvili N, Berthold P, Ollig D, Hegemann P, Bamberg E. Channelrhodopsin-2, a directly light-gated cation-selective membrane channel. Proc Natl Acad Sci. 2003;100(24):13940–5. Available from: http://www.pnas.org/cgi/doi/10.1073/pnas.1936192100

17. Boyden ES, Zhang F, Bamberg E, Nagel G, Deisseroth K. Millisecond-timescale, genetically targeted optical control of neural activity. Nat Neurosci. 2005 Aug 14;8:1263. Available from: http://dx.doi.org/10.1038/nn1525

18. Han X, Boyden ES. Multiple-Color Optical Activation , Silencing , and Desynchronization of Neural Activity , with Single-Spike Temporal Resolution. PLoS One. 2007;2(3).

19. Zhang F, Wang L-P, Brauner M, Liewald JF, Kay K, Watzke N, Wood PG, Bamberg E, Nagel G, Gottschalk A, Deisseroth K. Multimodal fast optical interrogation of neural circuitry. Nature. 2007 Apr 5;446:633. Available from: http://dx.doi.org/10.1038/nature05744

20. Cetin A, Komai S, Eliava M, Seeburg PH, Osten P. Stereotaxic gene delivery in the rodent brain. Nat Protoc. 2007 Jan 31;1:3166. Available from: http://dx.doi.org/10.1038/nprot.2006.450

21. Davidson BL, Breakefield XO. Viral vectors for gene delivery to the nervous system. Nat Rev Neurosci. 2003 May 1;4:353. Available from: http://dx.doi.org/10.1038/nrn1104

22. Carter M, Shieh J. Gene Delivery Strategies. In: Carter M, Shieh JBT-G to RT in N (Second E, editors. Guide to research techniques in neuroscience. second. San Diego: Academic Press; 2015. p. 239–52. Available from:

http://www.sciencedirect.com/science/article/pii/B9780128005118000113

23. Kohli V, Elezzabi AY. Laser surgery of zebrafish (Danio rerio) embryos using femtosecond laser pulses: Optimal parameters for exogenous material delivery, and the laser's effect on short- and long-term development. BMC Biotechnol. 2008;8:1–20.

24. Zeira E, Manevitch A, Khatchatouriants A, Pappo O, Hyam E, Darash-Yahana M, Tavor E, Honigman A, Lewis A, Galun E. Femtosecond infrared laser - An efficient and safe in vivo gene delivery system for prolonged expression. Mol Ther. 2003;8(2):342–50. Available from: http://dx.doi.org/10.1016/S1525-0016(03)00184-9

25. Guo Z V, Hart AC, Ramanathan S. Optical interrogation of neural circuits in Caenorhabditis elegans. Nat Methods. 2009 Nov 8;6:891. Available from: http://dx.doi.org/10.1038/nmeth.1397

26. Tian L, Hires SA, Mao T, Huber D, Chiappe ME, Chalasani SH, Petreanu L, Akerboom J, McKinney SA, Schreiter ER, Bargmann CI, Jayaraman V, Svoboda K, Looger LL. Imaging neural activity in worms, flies and mice with improved GCaMP calcium indicators. Nat Methods. 2009 Nov 8;6:875. Available from: http://dx.doi.org/10.1038/nmeth.1398

27. Scanziani M, Häusser M. Electrophysiology in the age of light. Nature. 2009 Oct 14;461:930. Available from: http://dx.doi.org/10.1038/nature08540

28. Bellmann D, Richardt A, Freyberger R, Nuwal N. Optogenetically induced olfactory stimulation in Drosophila larvae reveals the neuronal basis of odor-aversion behavior. Front Behav Neurosci. 2010;4(June):1–10.

29. Schroll C, Riemensperger T, Bucher D, Ehmer J, Vo T, Erbguth K, Gerber B, Hendel T, Nagel G, Buchner E. Light-Induced Activation of Distinct Modulatory Neurons Triggers Appetitive or Aversive Learning in Drosophila Larvae. Curr Biol. 2006;16:1741–7.

30. Hwang RY, Zhong L, Xu Y, Johnson T, Zhang F, Tracey WD. Nociceptive neurons protect Drosophila larvae from parasitoid wasps. Current. 2007;17(24):2105–16.

31. Xiang Y, Yuan Q, Vogt N, Looger LL, Jan LY, Jan YN. Light-avoidance-mediating photoreceptors tile the Drosophila larval body wall. Nature. 2010 Nov 10;468:921. Available from: http://dx.doi.org/10.1038/nature09576

32. Zhang W, Ge W, Wang Z. A toolbox for light control of Drosophila behaviors through Channelrhodopsin 2-mediated photoactivation of targeted neurons. Eur J Neurosci. 2007 Oct 26;26(9):2405–16. Available from: https://doi.org/10.1111/j.1460-

9568.2007.05862.x

33. Pulver SR, Pashkovski SL, Hornstein NJ, Garrity PA, Griffith LC. Temporal Dynamics of Neuronal Activation by Channelrhodopsin-2 and TRPA1 Determine Behavioral Output in Drosophila Larvae. J Neurophysiol. 2009 Jun 1;101(6):3075–88. Available from: http://www.ncbi.nlm.nih.gov/pmc/articles/PMC2694103/

34. Mclean DL, Fetcho JR. Movement , technology and discovery in the zebrafish. Curr Opin Neurobiol. 2011;21(1):110–5. Available from: http://dx.doi.org/10.1016/j.conb.2010.09.011

35. White RM, Sessa A, Burke C, Bowman T, Leblanc J, Ceol C, Bourque C, Dovey M, Goessling W, Burns CE, Zon LI. Transparent Adult Zebrafish as a Tool for In Vivo Transplantation Analysis. Cell Stem Cell. 2008;2(February):183–9.

36. Douglass AD, Kraves S, Deisseroth K, West CD. Escape Behavior Elicited by Single , Channelrhodopsin-2-Evoked Spikes in Zebrafish Somatosensory Neurons. Curr Biol. 2008;18:1133–7.

37. Zhu P, Narita Y, Bundschuh ST, Fajardo O, Schärer YZ, Chattopadhyaya B, Bouldoires EA, Stepien AE, Deisseroth K, Arber S, Sprengel R, Rijli FM, Friedrich RW, Friedrich RW, Miescher F. Optogenetic dissection of neuronal circuits in zebrafi sh using viral gene transfer and the Tet system. Front Neural Circuits. 2009;3(December):1–12.

38. Arenkiel BR, Peca J, Davison IG, Feliciano C, Deisseroth K, Augustine GJ, Ehlers MD, Feng G. In Vivo Light-Induced Activation of Neural Circuitry in Transgenic Mice Expressing Channelrhodopsin-2. Neuron. 2007;54:205–18.

39. Zhao S, Cunha C, Zhang F, Liu Q, Gloss B, Deisseroth K, Augustine GJ, Feng G. Improved expression of halorhodopsin for light-induced silencing of neuronal activity. Brain Cell Biol. 2008;36(1):141–54. Available from: https://doi.org/10.1007/s11068-008-9034-7

40. Sohal VS, Zhang F, Yizhar O, Deisseroth K. Parvalbumin neurons and gamma rhythms enhance cortical circuit performance. Nature. 2009 Apr 26;459:698. Available from: http://dx.doi.org/10.1038/nature07991

41. Hägglund M, Borgius L, Dougherty KJ, Kiehn O. Activation of groups of excitatory neurons in the mammalian spinal cord or hindbrain evokes locomotion. Nat Neurosci. 2010 Jan 17;13:246. Available from: http://dx.doi.org/10.1038/nn.2482

42. Kätzel D, Zemelman B V, Buetfering C, Wölfel M, Miesenböck G. The columnar and

laminar organization of inhibitory connections to neocortical excitatory cells. Nat Neurosci. 2010 Nov 14;14:100. Available from: http://dx.doi.org/10.1038/nn.2687

43. Thyagarajan S, Wyk M Van, Lehmann K, Lo S, Feng G, Wa H, Jena D-, Carolina N. Visual Function in Mice with Photoreceptor Degeneration and Transgenic Expression of Channelrhodopsin 2 in Ganglion Cells. J Neurosci. 2010;30(26):8745–58.

44. Covington HE, Lobo MK, Maze I, Vialou V, Hyman JM, Zaman S, Laplant Q, Mouzon E, Ghose S, Tamminga CA, Neve RL, Deisseroth K, Nestler EJ. Antidepressant Effect of Optogenetic Stimulation of the Medial Prefrontal Cortex. J Neurosci. 2010;30(48):16082–90.

45. Johansen JP, Hamanaka H, Mon MH, Behnia R, Deisseroth K, Blair HT. Optical activation of lateral amygdala pyramidal cells instructs associative fear learning. PNAS. 2010;107(28).

46. Ciocchi S, Herry C, Grenier F, Wolff SBE, Letzkus JJ, Vlachos I, Ehrlich I, Sprengel R, Deisseroth K, Stadler MB, Müller C, Lüthi A. Encoding of conditioned fear in central amygdala inhibitory circuits. Nature. 2010 Nov 10;468:277. Available from: http://dx.doi.org/10.1038/nature09559

47. Tye KM, Prakash R, Kim S, Fenno LE, Grosenick L, Zarabi H, Thompson KR, Gradinaru V, Ramakrishnan C. Amygdala circuitry mediating reversible and bidirectional control of anxiety. Nature. 2011;471(7338):358–62.

48. Han X, Qian X, Bernstein JG, Zhou H, Franzesi GT, Stern P, Bronson RT, Graybiel AM, Desimone R, Boyden ES. Millisecond-Timescale Optical Control of Neural Dynamics in the Nonhuman Primate Brain. Neuron. 2009;62(2):191–8. Available from: http://dx.doi.org/10.1016/j.neuron.2009.03.011

49. Diester I, Kaufman MT, Mogri M, Pashaie R, Goo W, Yizhar O, Ramakrishnan C, Deisseroth K, Shenoy K V. An optogenetic toolbox designed for primates. Nat Neurosci. 2011 Jan 30;14:387. Available from: http://dx.doi.org/10.1038/nn.2749

50. Busskamp V, Duebel J, Balya D, Fradot M, Viney TJ, Siegert S, Groner AC, Cabuy E, Forster V, Seeliger M, Biel M, Humphries P, Paques M, Mohand-Said S, Trono D, Deisseroth K, Sahel JA, Picaud S, Roska B. Genetic Reactivation of Cone Photoreceptors Restores Visual Responses in Retinitis Pigmentosa. Science (80-). 2010 Jul 23;329(5990):413 LP-417. Available from: http://science.sciencemag.org/content/329/5990/413.abstract

51. Levitz J, Pantoja C, Gaub B, Janovjak H, Reiner A, Hoagland A, Schoppik D, Kane B,

Stawski P, Schier AF, Trauner D, Isacoff EY. Optical control of metabotropic glutamate receptors. Nat Neurosci. 2013;16(4):507–16. Available from: http://www.pubmedcentral.nih.gov/articlerender.fcgi?artid=3681425&tool=pmcentrez&rendertype=abstract

52. Levitz J, Popescu AT, Reiner A, Isacoff EY. A Toolkit for Orthogonal and in vivo Optical Manipulation of Ionotropic Glutamate Receptors. Front Mol Neurosci. 2016;9(February):1–15. Available from: http://journal.frontiersin.org/Article/10.3389/fnmol.2016.00002/abstract

53. Banghart M, Borges K, Isacoff E, Trauner D, Kramer RH. Light-activated ion channels for remote control of neuronal firing. Nat Neurosci. 2004 Nov 21;7:1381. Available from: http://dx.doi.org/10.1038/nn1356

54. Heginbotham L, Mackinnon R. Conduction Properties of the Cloned Shaker K + Channel. 1993;65(November):2089–96.

55. Chambers JJ, Banghart MR, Trauner D, Kramer RH. Light-Induced Depolarization of Neurons Using a Modified Shaker K+ Channel and a Molecular Photoswitch. J Neurophysiol. 2006;96(5):2792–6. Available from: http://jn.physiology.org/cgi/doi/10.1152/jn.00318.2006

56. Heginbotham L, Lu Z, Abramson T, MacKinnon R. Mutations in the K+ channel signature sequence. Biophys J. 1994;66(4):1061–7.

57. Kandel ER, Schwartz JH, Jessell TM, Jessell D of B and MBT, Siegelbaum S, Hudspeth AJ. Principles of neural science. Vol. 4. McGraw-hill New York; 2000.

58. Banghart MR, Volgraf M, Trauner D. Engineering Light-Gated Ion Channels. Biochemistry. 2006 Dec 1;45(51):15129–41. Available from: https://doi.org/10.1021/bi0618058

59. Mayer ML. Glutamate receptors at atomic resolution. Nature. 2006 Mar 22;440:456. Available from: http://dx.doi.org/10.1038/nature04709

60. Mayer ML. Crystal structures of the GluR5 and GluR6 ligand binding cores: Molecular mechanisms underlying kainate receptor selectivity. Neuron. 2005;45(4):539–52.

61. Jin R, Banke TG, Mayer ML, Traynelis SF, Gouaux E. Structural basis for partial agonist action at ionotropic glutamate receptors. Nat Neurosci. 2003 Jul 20;6:803. Available from: http://dx.doi.org/10.1038/nn1091

62. Hille B. Ion Channel Excitable Membranes. Sunderland Massachusetts USA. 2001. p. 1–

37.

63. Burnashev N, Villarroel A, Sakmann B. Dimensions and ion selectivity of recombinant AMPA and kainate receptor channels and their dependence on Q / R site residues exp (Vrev ,/ RT)) I Vrv = RT InaCso. 1996;165–73.

64. Li G, Oswald RE, Niu L. Channel-Opening Kinetics of GluR6 Kainate Receptor. Biochemistry. 2003 Oct 1;42(42):12367–75. Available from: https://doi.org/10.1021/bi034797t

65. Swanson GT, Feldmeyer D, Kaneda M, Cull-Candy SG. Effect of RNA editing and subunit co-assembly on single-channel properties of recombinant kainate receptors. J Physiol. 1996;492(1):129–42.

66. Gorostiza P, Volgraf M, Numano R, Szobota S, Trauner D, Isacoff EY. Mechanisms of photoswitch conjugation and light activation of an ionotropic glutamate receptor. Proc Natl Acad Sci U S A. 2007;104(26):10865–70.

67. Reiner A, Isacoff EY. Tethered ligands reveal glutamate receptor desensitization depends on subunit occupancy. Nat Chem Biol. 2014;10(4):273–80. Available from: http://www.ncbi.nlm.nih.gov/pubmed/24561661

68. Szobota S, Gorostiza P, Del Bene F, Wyart C, Fortin DL, Kolstad KD, Tulyathan O, Volgraf M, Numano R, Aaron HL, Scott EK, Kramer RH, Flannery J, Baier H, Trauner D, Isacoff EY. Remote Control of Neuronal Activity with a Light-Gated Glutamate Receptor. Neuron. 2007;54(4):535–45.

69. Hou Q, Gilbert J, Man H. Homeostatic regulation of AMPA receptor trafficking and degradation by light-controlled single synpatic activation. Neuron. 2011;(72(5)):806–18.

70. Numano R, Szobota S, Lau AY, Gorostiza P, Volgraf M, Roux B, Trauner D, Isacoff EY. Nanosculpting reversed wavelength sensitivity into a photoswitchable iGluR. Proc Natl Acad Sci U S A. 2009;106(16):6814–9.

71. Janovjak H, Szobota S, Wyart C, Trauner D, Ehud Y. A light-gated, potassium-selective glutamate receptor for the optical inhibition of neuronal firing. 2011;13(8):1027–32.

72. Kienzler MA, Reiner A, Trautman E, Yoo S, Trauner D, Isacoff EY. A Red-Shifted, Fast-Relaxing Azobenzene Photoswitch for Visible Light Control of an Ionotropic Glutamate Receptor. J Am Chem Soc. 2013 Nov 27;135(47):17683–6. Available from: https://doi.org/10.1021/ja408104w

73. Izquierdo-Serra M, Gascón-Moya M, Hirtz JJ, Pittolo S, Poskanzer KE, Ferrer È, Alibés

R, Busqué F, Yuste R, Hernando J, Gorostiza P. Two-Photon Neuronal and Astrocytic Stimulation with Azobenzene-Based Photoswitches. J Am Chem Soc. 2014 Jun 18;136(24):8693–701. Available from: https://doi.org/10.1021/ja5026326

74. Carroll EC, Berlin S, Levitz J, Kienzler MA, Yuan Z, Madsen D, Larsen DS, Isacoff EY. Two-photon brightness of azobenzene photoswitches designed for glutamate receptor optogenetics. Proc Natl Acad Sci. 2015 Feb 17;112(7):E776 LP-E785. Available from: http://www.pnas.org/content/112/7/E776.abstract

75. Lin JY. A User's Guide to Channelrhodopsin Variants. Exp Physiol. 2012;96(1):19–25.

76. Feldbauer K, Zimmermann D, Pintschovius V, Spitz J, Bamann C, Bamberg E. Channelrhodopsin-2 is a leaky proton pump. Proc Natl Acad Sci U S A. 2009;106(30):12317–22. Available from: http://www.pubmedcentral.nih.gov/articlerender.fcgi?artid=2718366&tool=pmcentrez&rendertype=abstract

77. Dulhunty AF. Excitation-contraction coupling from the 1950s to the new millenium. Clin Exp Pharmacol Physiol. 2006;(April):763–72.

78. Lu KP, Means AR. Regulation of the Cell Cycle by Calcium and Calmodulin. Endocr Rev. 1993 Feb 1;14(1):40–58. Available from: http://dx.doi.org/10.1210/edrv-14-1-40

79. Orrenius S, Zhivotovsky B, Nicotera P. Regulation of cell death: The calcium-apoptosis link. Nat Rev Mol Cell Biol. 2003;4(7):552–65.

80. Berridge MJ, Lipp P, Bootman MD. The versatility and universality of calcium signalling. Nat Rev Mol Cell Biol. 2000 Oct 1;1:11. Available from: http://dx.doi.org/10.1038/35036035

81. Bootman MD, Rietdorf K, Collins T, Walker S, Sanderson M. Ca2+-Sensitive Fluorescent Dyes and Intracellular Ca2+ Imaging. Cold Spring Harb Protoc. 2013;2013(2):pdb.top066050-pdb.top066050. Available from: http://www.cshprotocols.org/cgi/doi/10.1101/pdb.top066050

82. Grienberger C, Konnerth A. Imaging Calcium in Neurons. Neuron. 2012;73(5):862–85. Available from: http://dx.doi.org/10.1016/j.neuron.2012.02.011

83. Neher E, Sakaba T. Multiple Roles of Calcium Ions in the Regulation of Neurotransmitter Release. Neuron. 2008;59(6):861–72.

84. Zucker R. Calcium- and activity-dependent synaptic plasticity. Vol. 9, Current Opinion in Neurobiology. 1999. 305-313 p.

85. Lyons MR, West AE. Mechanisms of specificity in neuronal activity-regulated gene transcription. Prog Neurobiol. 2011 Aug 1;94(3):259–95. Available from: https://www.sciencedirect.com/science/article/pii/S0301008211000748?via%3Dihub

86. Berridge MJ, Bootman MD, Roderick HL. Calcium signalling: dynamics, homeostasis and remodelling. Nat Rev Mol Cell Biol. 2003 Jul 1;4:517. Available from: http://dx.doi.org/10.1038/nrm1155

87. Clapham DE. Calcium Signaling. Cell. 2007;131(6):1047–58.

88. Fucile S. Ca2+ permeability of nicotinic acetylcholine receptors. Cell Calcium. 2004 Jan 1;35(1):1–8. Available from: https://www.sciencedirect.com/science/article/pii/S0143416003001854

89. Higley MJ, Sabatini BL. Calcium Signaling in Dendrites and Spines: Practical and Functional Considerations. Neuron. 2008 Sep 25;59(6):902–13. Available from: https://www.sciencedirect.com/science/article/pii/S0896627308007447

90. Ramsey IS, Delling M, Clapham DE. AN INTRODUCTION TO TRP CHANNELS. Annu Rev Physiol. 2006 Jan 1;68(1):619–47. Available from: https://doi.org/10.1146/annurev.physiol.68.040204.100431

91. Duchen MR. Contributions of mitochondria to animal physiology: From homeostatic sensor to calcium signalling and cell death. J Physiol. 1999;516(1):1–17.

92. Berridge MJ. Neuronal Calcium Signaling. Neuron. 1998;21:13–26.

93. Paredes RM, Etzler JC, Watts LT, Lechleiter JD. Chemical Calcium Indicators. Methods. 2008;46(3):143–51.

94. Lipp P, Lüscher C, Niggli E. Photolysis of caged compounds characterized by ratiometric confocal microscopy : A new approach to homogeneously control and measure the calcium concentration in cardiac myocytes. Cell Calcium. 1996;255–66.

95. Nicotera P, Rossi AD. Nuclear Ca 2+ : physiological regulation and role in apoptosis. Mol Cell Biochem. 1994;135:89–98.

96. Schild D, Jung A, Schultens HA. Localization of calcium entry through calcium channels in olfactory receptor neurones using a laser scanning microscope and the calcium indicator dyes Fluo-3 and Fura-Red. Cell Calcium. 1994;15(5):341–8. Available from: http://www.sciencedirect.com/science/article/pii/0143416094900094

97. Paredes RM, Etzler JC, Watts LT, Zheng W, Lechleiter JD. Chemical calcium indicators. Methods. 2008;46(3):143–51. Available from:

http://dx.doi.org/10.1016/j.ymeth.2008.09.025

98. Bozza T, McGann JP, Mombaerts P, Wachowiak M. In vivo imaging of neuronal activity by targeted expression of a genetically encoded probe in the mouse. Neuron. 2004;42(1):9–21.

99. Mao T, O'Connor DH, Scheuss V, Nakai J, Svoboda K. Characterization and subcellular targeting of GCaMP-type genetically-encoded calcium indicators. PLoS One. 2008;3(3):1–10.

100. Shigetomi E, Kracun S, Sofroniew M V., Khakh BS. A genetically targeted optical sensor to monitor calcium signals in astrocyte processes. Nat Neurosci. 2010;13(6):759–66. Available from: http://dx.doi.org/10.1038/nn.2557

101. Luo L, Callaway EM, Svoboda K. Genetic Dissection of Neural Circuits. Neuron. 2008;57(5):634–60.

102. Wang Q, Shui B, Kotlikoff MI, Sondermann H. Structural Basis for Calcium Sensing by GCaMP2. Structure. 2008;16(12):1817–27. Available from: http://dx.doi.org/10.1016/j.str.2008.10.008

103. Akerboom J, Rivera JDV, Rodríguez Guilbe MM, Malavé ECA, Hernandez HH, Tian L, Hires SA, Marvin JS, Looger LL, Schreiter ER. Crystal structures of the GCaMP calcium sensor reveal the mechanism of fluorescence signal change and aid rational design. J Biol Chem. 2009;284(10):6455–64.

104. Pérez Koldenkova V, Nagai T. Genetically encoded Ca 2+ indicators : Properties and evaluation. BBA - Mol Cell Res. 2013;1833(7):1787–97. Available from: http://dx.doi.org/10.1016/j.bbamcr.2013.01.011

105. Nakai J, Ohkura M, Imoto K. A high signal-to-noise Ca2+ probe composed of a single green fluorescent protein. Nat Biotechnol. 2001 Feb 1;19:137. Available from: http://dx.doi.org/10.1038/84397

106. Lakowicz JR. Principles of Fluorescence Spectroscopy. third. Springer US; 2006.

107. Nagai T, Yamada S, Tominaga T, Ichikawa M, Miyawaki A. Expanded dynamic range of fluorescent indicators for Ca2+ by circularly permuted yellow fluorescent proteins. Proc Natl Acad Sci U S A. 2004 Jul 20;101(29):10554 LP-10559. Available from: http://www.pnas.org/content/101/29/10554.abstract

108. Palmer AE, Tsien RY. Measuring calcium signaling using genetically targetable fluorescent indicators. Nat Protoc. 2006;1(3):1057–65.

109. Rehberg M, Lepier A, Solchenberger B, Osten P, Blum R. A new non-disruptive strategy to target calcium indicator dyes to the endoplasmic reticulum. Cell Calcium. 2008;44(4):386–99.

110. Andermann ML. Chronic cellular imaging of mouse visual cortex during operant behavior and passive viewing. Front Cellullar Neurosci. 2010;4(March):1–16. Available from: http://journal.frontiersin.org/article/10.3389/fncel.2010.00003/abstract

111. Mank M, Santos AF, Direnberger S, Mrsic-Flogel TD, Hofer SB, Stein V, Hendel T, Reiff DF, Levelt C, Borst A, Bonhoeffer T, Hübener M, Griesbeck O. A genetically encoded calcium indicator for chronic in vivo two-photon imaging. Nat Methods. 2008;5(9):805–11.

112. Yamagata K, Iwamoto D, Terashita Y, Li C, Wakayama S. Fluorescence Cell Imaging and Manipulation Using Conventional Halogen Lamp Microscopy. 2012;7(2).

ACKNOWLEDGEMENTS

First of all, I would like to thank my supervisor Professor Vincent Torre for his help and guidance during my PhD.

I would also like to thank Dr. Andrea Barberis and his laboratory members for the kindest hospitality during my visit at IIT. Thank you for your time and for your invaluable insights.

My gratitude also goes to Dr. Ulisse Bocchero, my friend and colleague with whom I shared this adventure. Thank you for your friendship and support, and for teaching me how to splice and taper optical fibres!

Thank you to my dear friend Francesca, for being by my side since the very beginning of this journey in Trieste. A great thank you goes to all my closest friends, both here and back home. Distance really doesn't mean a thing.

Thank you Marco, for the support, the love, the laughs, the time spent together, for always being there. Thank you for everything.

And last but not least, I dedicate this thesis to my family. Mamma, Babbo e Angelo, non potrò mai ringraziarvi abbastanza per il vostro sostegno e per il costante incoraggiamento.